Hawke's Bay 3D Aquifer Mapping Project:

3D hydrogeological models from SkyTEM data in the Ruataniwha Plains

January 2024
Hawkes Bay Regional Council Publication No. 5633

HAWKES BAY REGIONAL COUNCIL
TE KAUNIHERA Ā-ROHE O TE MATAU-A-MĀUI

ISSN 2703-2051 (Online)
ISSN 2703-2043 (Print)

HAWKES BAY REGIONAL COUNCIL
TE KAUNIHERA Ā-ROHE O TE MATAU-A-MĀUI

(06) 835 9200
0800 108 838
Private Bag 6006 Napier 4142
159 Dalton Street . Napier 4110

Environmental Science

Hawke's Bay 3D Aquifer Mapping Project:

3D hydrogeological models from SkyTEM data in the Ruataniwha Plains

January 2024
Hawkes Bay Regional Council Publication No. 5633

Prepared By:

GNS Science

ZJ Rawlinson

For: Hawke's Bay Regional Council

Reviewed by:
S Harper, Hawke's Bay Regional Council
T Wilson, Hawke's Bay Regional Council
M Herpe, GNS Science
TR Sahoo, GNS Science
SG Cameron, GNS Science

.

ISSN 2703-2051 (Online)
ISSN 2703-2043 (Print)

Hawke's Bay 3D Aquifer Mapping Project: 3D hydrogeological models from SkyTEM data in the Ruataniwha Plains

ZJ Rawlinson

GNS Science Consultancy Report 2023/117
January 2024

GNS SCIENCE
TE PŪ AO

DISCLAIMER

This report has been prepared by the Institute of Geological and Nuclear Sciences Limited (GNS Science) exclusively for and under contract to Hawke's Bay Regional Council. Unless otherwise agreed in writing by GNS Science, GNS Science accepts no responsibility for any use of or reliance on any contents of this report by any person other than Hawke's Bay Regional Council and shall not be liable to any person other than Hawke's Bay Regional Council, on any ground, for any loss, damage or expense arising from such use or reliance.

Use of Data:

Date that GNS Science can use associated data: January 2024

BIBLIOGRAPHIC REFERENCE

Rawlinson ZJ. 2024. Hawke's Bay 3D Aquifer Mapping Project: 3D hydrogeological models from SkyTEM data in the Ruataniwha Plains. Lower Hutt (NZ): GNS Science. 60 p. Consultancy Report 2023/117.

CONTENTS

FIGURES

TABLES

EXECUTIVE SUMMARY

This report synthesises and analyses information from the previous Ruataniwha Plains reports produced by the Hawke's Bay 3D Aquifer Mapping Project (3DAMP). The primary objective of this report is to provide detailed 3D models and hydrogeological interpretations suitable to be utilised by subsequent numerical modelling and online visualisation tools. A further objective is to develop a refined understanding of near-surface permeability relevant to groundwater-surface water interaction.

Previous information this report synthesises includes: SkyTEM data; resistivity models; datasets collected during the drilling of 3DAMP_Well1 and 3DAMP_Well3; a data and model inventory report; a high-quality/deep borehole interpretation report; manual delineation of major hydrogeological units; and automated hydrostratigraphic modelling. It is beyond the scope of this report to inspect small subsets of these data at the local scale. Here, the entire volume of data was assessed at the catchment scale, which necessitated a methodology that could handle the inspection of a large amount of data. In the future, local studies could refine models through closer interrogation and refinement of datasets for specific local applications.

A series of 3D models were developed with 100 x 100 m grid cells horizontally and 2-m-thick grid cells vertically. The 3D models developed are as follows:

- An interpolated resistivity (res) model.
- A major Hydrogeological Unit (HU) model.
- A Hydrostratigraphic (HS) model.
- A resistivity facies (facies) model.
- An Aquifer Potential (AP) model.
- A Coarse fraction Classification model (CC).
- Horizontal Hydraulic Conductivity models (KH).

2D maps/models were also derived, primarily using the CC model:

- Aquifer thickness, separated into surficial, deep, total thickness and total thickness as a percentage of unconsolidated thickness.
- Aquitard thickness.
- Near-surface properties (res, CC and KH) for the upper 5 m, 10 m, 15 m, 20 m, 30 m and 50 m, using the geometric and harmonic mean.
- Geometric and harmonic mean of horizontal hydraulic conductivity (KH) through the full vertical column of unconsolidated sediments and consolidated sediments where these outcrop at the surface.

3D model datasets were created and saved in an accessible *.csv* format, with x,y,z defining the centre of each grid cell. This format enables rapid model visualisation in an interactive online webmap and as 3D block models within a Leapfrog software viewer file. A selection of these models was also converted to multi-band raster format, enabling further accessibility such as visualisation of elevation slices within GIS software. 2D models were developed in raster format, with some simplified to polygon shapefiles where appropriate.

Simplifications of the 3D models to 2D maps assisted with investigating various aspects of the Ruataniwha Plains groundwater system, and with comparisons to previous investigations, highlighting the benefits of these datasets. Overall, the maps and models developed provide useful information to improve the understanding of the hydrogeological system in the Ruataniwha Plains, support a greater understanding of other datasets (e.g. from pumping tests and stream flow gaugings), and could be used to guide additional data collection with greater precision.

This page left intentionally blank.

1.0 INTRODUCTION

This report synthesises and analyses information from the previous Ruataniwha Plains reports produced by the Hawke's Bay 3D Aquifer Mapping Project (3DAMP). The primary objective of this report is to provide detailed 3D models and hydrogeological interpretations suitable to be utilised by subsequent numerical modelling and online visualisation tools. A further objective is to develop a refined understanding of near-surface permeability relevant to groundwater-surface water interaction.

3DAMP is a four-year initiative (2019–2023) jointly funded by the Provincial Growth Fund (PGF), Hawke's Bay Regional Council (HBRC) and GNS Science's (GNS) Groundwater Strategic Science Investment Fund (SSIF) research programme. The project applies SkyTEM technology to improve mapping and modelling of groundwater resources within the Heretaunga Plains, Ruataniwha Plains and Poukawa and Ōtāne basins. 3DAMP involves collaboration between HBRC, GNS and the Aarhus University HydroGeophysics Group (HGG).

Previous information this report synthesises includes:

- SkyTEM data (SkyTEM Australia 2020).
- SkyTEM-derived resistivity models (Rawlinson et al. 2022).
- Datasets collected during the drilling of 3DAMP_Well1 and 3DAMP_Well3 (Lawrence et al. 2022a, 2022b).
- A data and model inventory report (Tschritter et al. 2022).
- A high-quality/deep borehole interpretation report (Kellett et al. 2023).
- Manual delineation of major hydrogeological units (Sahoo et al. 2023).
- Automated hydrostratigraphic modelling (Herpe and Rawlinson 2023).

1.1 Objectives

The objectives of this report include both dataset creation and assessments related to hydrogeological interpretation within the Ruataniwha model area (Figure 1.1).

Hydrogeological interpretation of resistivity models is a process of translating resistivity values (typically represented by the unit ohm.m or Ω·m) to categorical or numerical values of more immediate use to a hydrogeologist. The numerical values present in a resistivity model are a function of complex relationships between porosity, permeability, grain size and sorting, mineralogical content such as clay, and fluid properties (e.g. Figure 1.2). Supporting local information (e.g. lithological logs) is therefore required to interpret the resistivity models.

The primary objectives are as follows:

- Develop datasets suitable for display within an online 3D model visualisation tool.
- Develop datasets suitable for use within numerical groundwater models, for example, hydraulic property information relevant for numerical groundwater modelling implementation.
- Develop datasets that describe near-surface permeability, which is relevant to groundwater–surface water interaction.

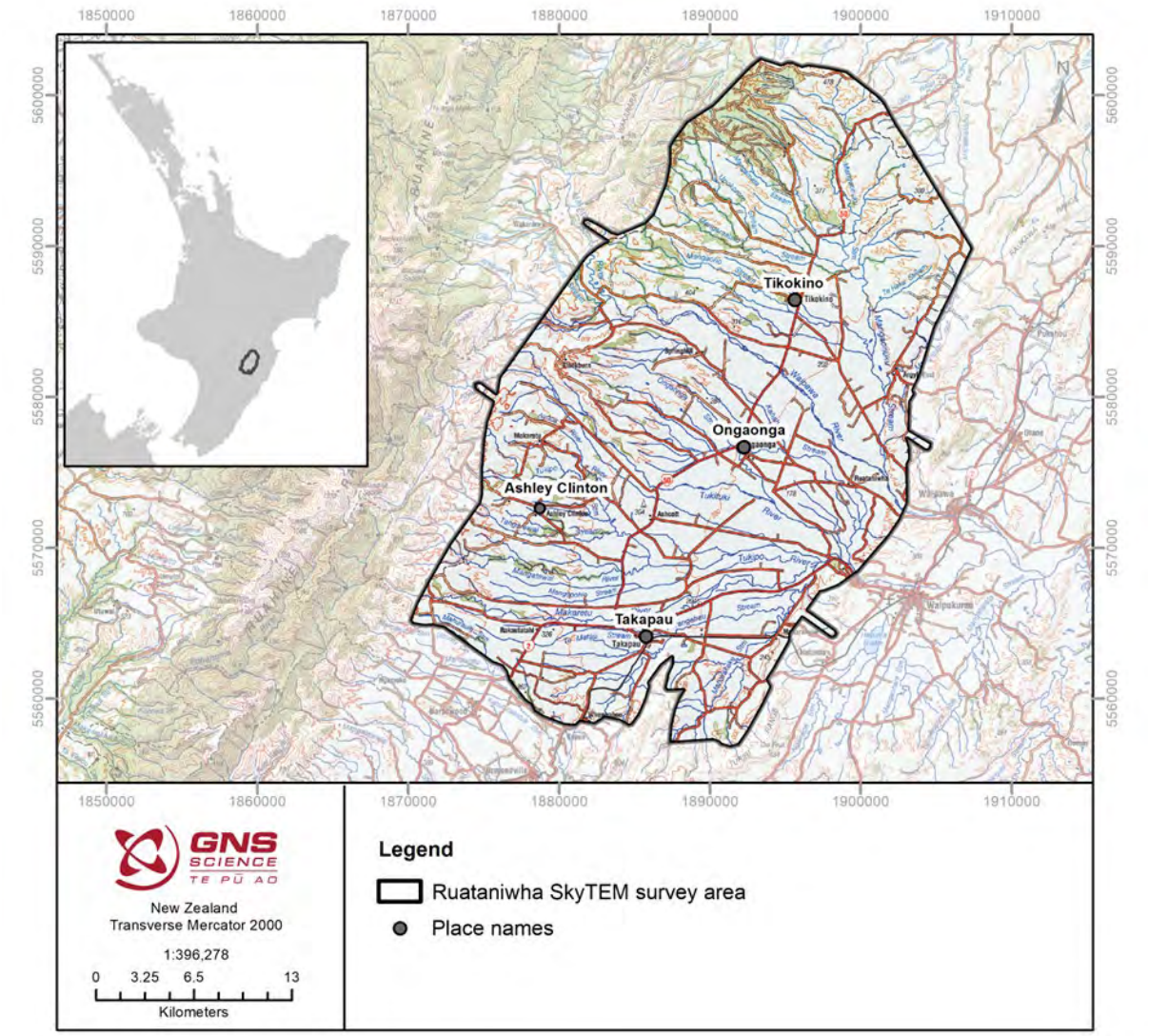

Figure 1.1 Location map of the Ruataniwha Plains showing the extent of the SkyTEM survey area (Ruataniwha model area). Figure and caption from Tschritter et al. (2022).

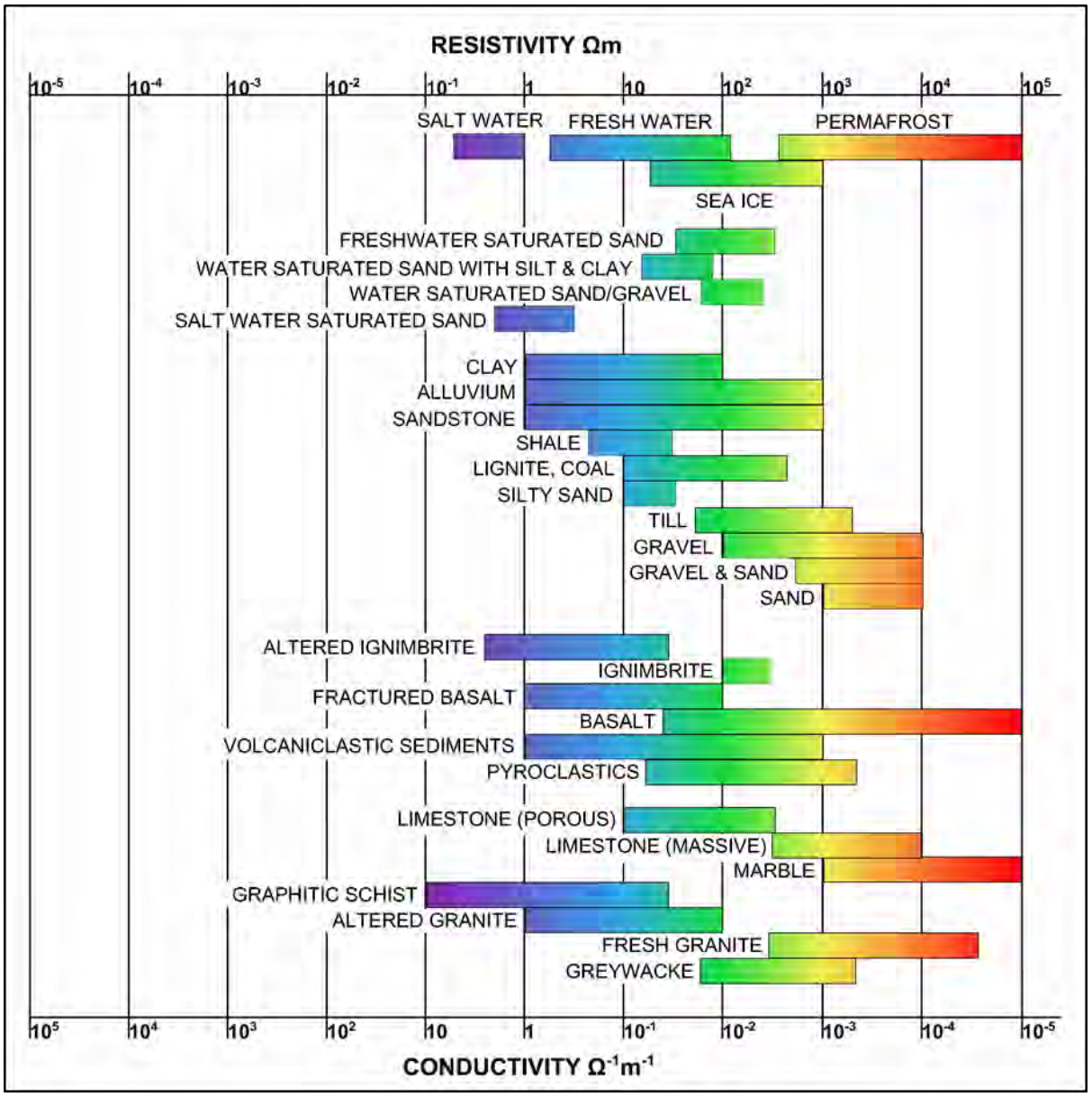

Figure 1.2 Ranges of electrical resistivity for some common lithologies measured in-situ, compiled from a variety of publications. Figure from Rawlinson (2013).

2.0 METHOD

The resistivity models (Rawlinson et al. 2022) consist of a large amount of data: greater than three million data points in each resistivity model. It is beyond the scope of this report to inspect small subsets of these data at the local scale. Here, the entire volume of data is assessed at the catchment scale, which necessitates a methodology that can handle the inspection of a large amount of data.

To manage the assessment of this amount of data, as well as the relatively sparse supporting datasets, a combined approach of manual and automated methods for interpretation was utilised. In previous work, Kellett et al. (2023) and Sahoo et al. (2023) largely utilised manual methodologies of interpretation, while Herpe and Rawlinson (2023) utilised a largely automated approach. This section describes how these previous pieces of work have been combined into 3D and 2D datasets that can then be used in various hydrogeological applications, and follows the methodology developed in Rawlinson (2023).

2.1 3D-Gridded Model Development

In this section, 3D models suitable for numerical groundwater modelling and online visualisation were developed.

The resistivity model datasets developed by Rawlinson et al. (2022) are 1D models at SkyTEM data locations (Figure 2.1). These datasets are essentially point datasets that include gaps where electromagnetic noise was removed and where the helicopter was unable to fly due to flight path restrictions. These datasets were interpolated to a 3D grid with horizontal cell resolution of 100 m (Figure 2.2) and vertical resolution of 2 m.

The previous data and model inventory report and associated datasets (Tschritter et al. 2022; e.g. borehole lithological information, water levels and previous conceptual understanding and models) were used extensively to guide 3D and 2D model development. Results are displayed along the cross-section shown in Figure 2.1.

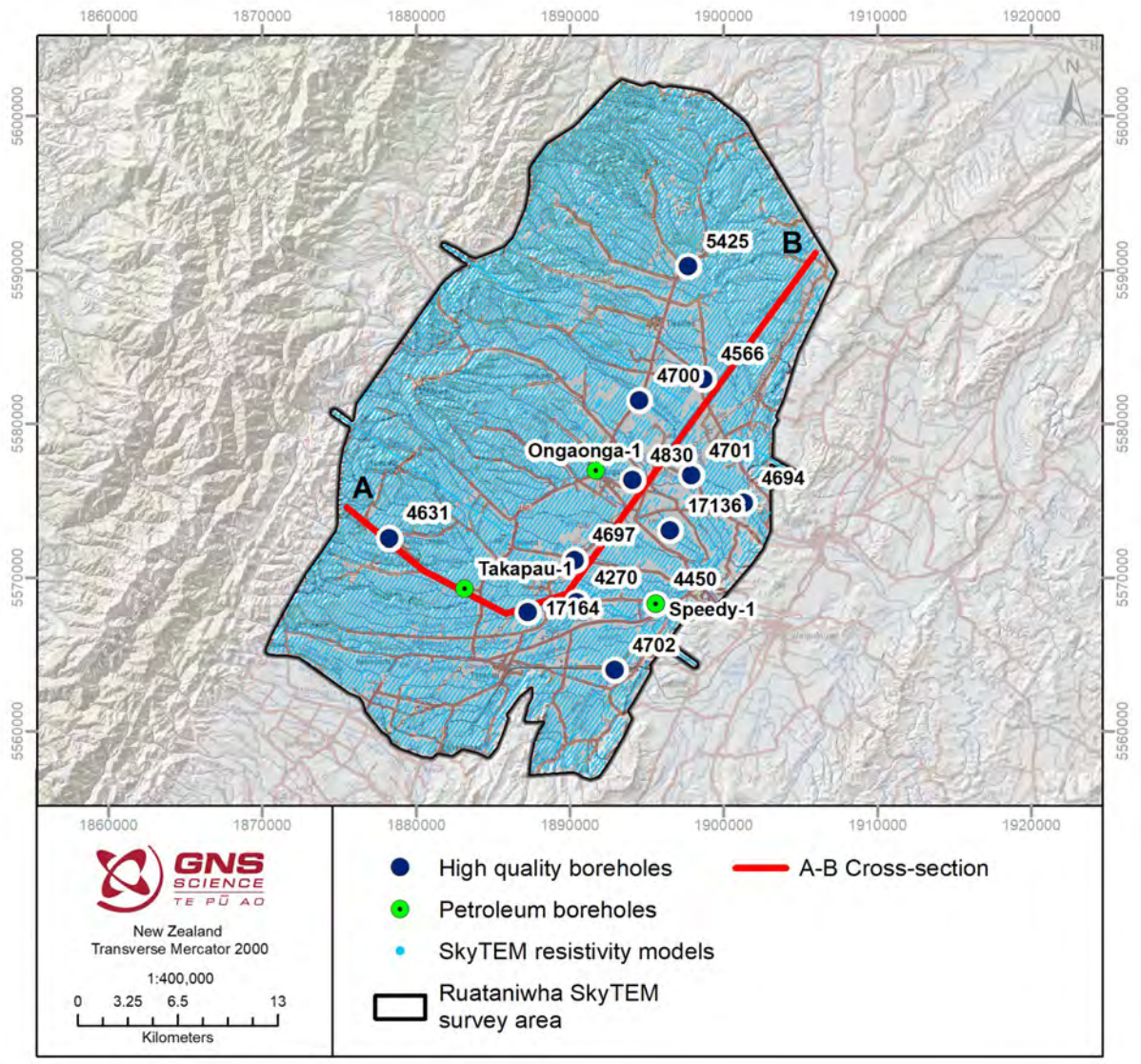

Figure 2.1 Location of SkyTEM-derived 1D resistivity models in the Ruataniwha Plains. Also shown are deep wells with high-quality lithological logs utilised by Kellet et al. (2023). Cross-sections were prepared through A-B to display results.

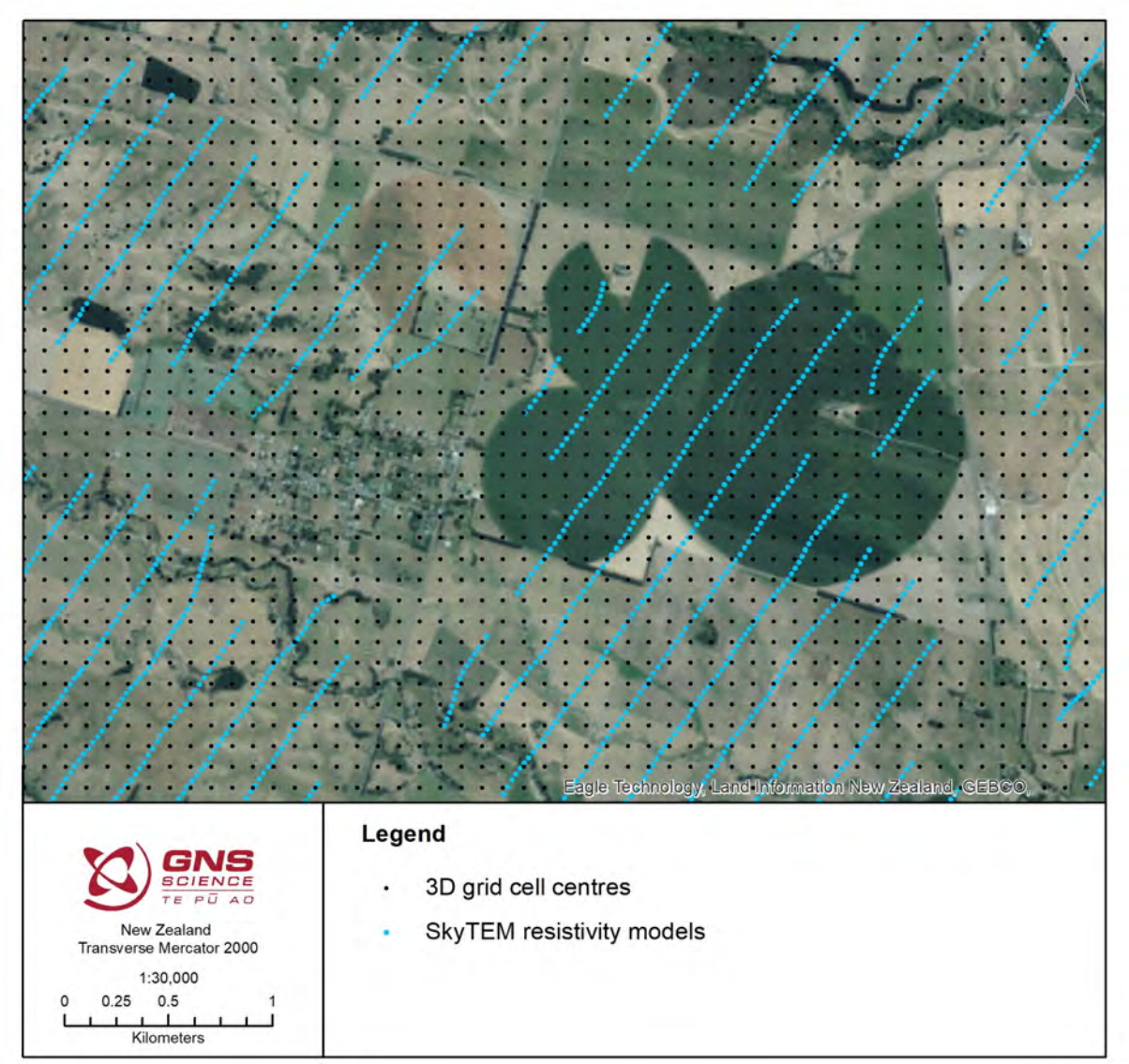

Figure 2.2 Small section of the Ruataniwha model area showing the difference between the original SkyTEM resistivity model locations along flight lines and the 3D uniformly gridded model locations (100 m horizontal resolution).

2.1.1 Interpolated Resistivity (res) Model

To develop a more continuous 3D dataset, interpolation of the resistivity values to a uniform 3D grid was undertaken using Geoscene3D software (IGIS 2023).

Historical resistivity data provided valuable information in some of the gaps within the SkyTEM data (Figure 2.3; Tschritter et al. 2022). As multiple datasets are not able to be combined during interpolation within Geoscene3D software, the 1D layered resistivity model datasets were combined by re-sampling them as x,y,z locations with a maximum of 5 m vertical separation between x,y,z points (i.e. re-sampling thicker layers) and exporting the combined dataset as a single *.csv* file. Where depth of investigation (DOI[1]) calculations were available (e.g. Figure 2.4), data below 'DOI_Standard' were not included in this combined dataset.

[1] For each resistivity model, DOI was previously estimated. The DOI calculation takes into account the SkyTEM system transfer function, the number of data points, the data uncertainty and the resistivity model. Resistivity structures below the DOI standard value are very weakly determined by the data (Rawlinson et al. 2021).

This ensures that resistivity data with higher uncertainty values are not used in the interpolation. The following datasets were combined (described further within Tschritter et al. [2022]):

- SkyTEM (airborne Time-domain ElectroMagnetic) data:
  - *Ruataniwha_smooth_resistivitymodel_V1_2022_inv.xyz*
- GroundTEM (Ground-based Time-domain ElectroMagnetic) data. Where both were present, the NanoTEM and TEM results were merged into a single 1D sounding, preferentially using the NanoTEM results in the upper 50 m.
  - *Ruataniwha_TEMnanoTEM_2009.csv*
  - *Ruataniwha_TEMnanoTEM_20192021.csv*

Smooth models were chosen for this combination, as they were available for all the datasets and provide finer detail than the sharp models[2].

These data were imported as a point dataset into Geoscene3D. This point dataset shows a roughly Gaussian distribution when transformed into $\log_{10}$ space (Figure 2.5), so Kriging was selected as appropriate for interpolation. Kriging also provides a corresponding 3D grid with an interpolation uncertainty estimate (the kriging variance), which could be utilised within subsequent applications such as numerical groundwater modelling.

A uniform 3D grid was defined with 100 x 100 m horizontal resolution and 2 m vertical resolution (cell thickness), matching the extents of the resistivity data. The large memory footprint of the dataset prevented generation of a finer resolution 3D grid at this full extent.

Geoscene3D software uses the GSLIB kriging library. Interpolation was undertaken on the $\log_{10}$-transformed resistivity data. A number of tests were performed on various smaller selections of data to check for the most appropriate kriging variables. Point Kriging was undertaken using a spherical function, sill of 0.1 and range of 2000 m. A 500 m horizontal search radius, 25 m vertical search radius and maximum of six data points in each octant were used. The horizontal and vertical search radii used impact the final coverage of the dataset.

Once interpolation was completed, null values were assigned to grid nodes outside the Ruataniwha model area and above the Digital Elevation Model (DEM) (25 m resolution, as utilised within Sahoo et al. [2023]). The gridded resistivity model was exported as a *.csv* file, which consists of resistivity values mapped to cell nodes *X, Y, Z,* and *res*. The kriging variance gridded model was similarly exported to a *.csv* file including the following: *X, Y, Z, resvar*.

Upon inspection of the interpolated resistivity model, a small anomalous low-resistive area was apparent in the near-surface. Near-surface low-resistivity features can be caused by EM noise still present in the dataset. This location was cross-checked against the QC maps in Rawlinson et al. (2022), and two data points were identified with high data residuals near a major powerline. Although all efforts were made to remove EM noise during SkyTEM data

[2] A smooth model is a many-layered model that uses a fixed layer structure (logarithmically increasing layer thicknesses), and the resistivity of each layer is solved for. The smooth regularisation scheme penalises the resistivity changes, resulting in the smoothest resistivity transitions both vertically and horizontally. A sharp model uses the same model discretisation as the smooth model, but the model regularisation scheme is different. The sharp model regularisation scheme penalises the number of resistivity changes above a certain size, instead of the absolute resistivity changes (as in the smooth model regularisation scheme). The sharp model regularisation scheme therefore results in a model with few, but relatively sharp resistivity transitions. This allows for relative abrupt changes in resistivities, while using the fixed layer thicknesses of the smooth model (e.g. Rawlinson et al. 2022).

processing, it appears that these two points are still contaminated by EM noise, which was highlighted through the kriging interpolation process. The associated data points were removed ([Easting, Northing] = [1899088.125, 5579937.00] and [Easting, Northing] = [1899068.00, 5579910.00]) and the above kriging procedure repeated. Upon inspection of the resulting interpolated resistivity model, the anomalous low-resistive feature had successfully been removed.

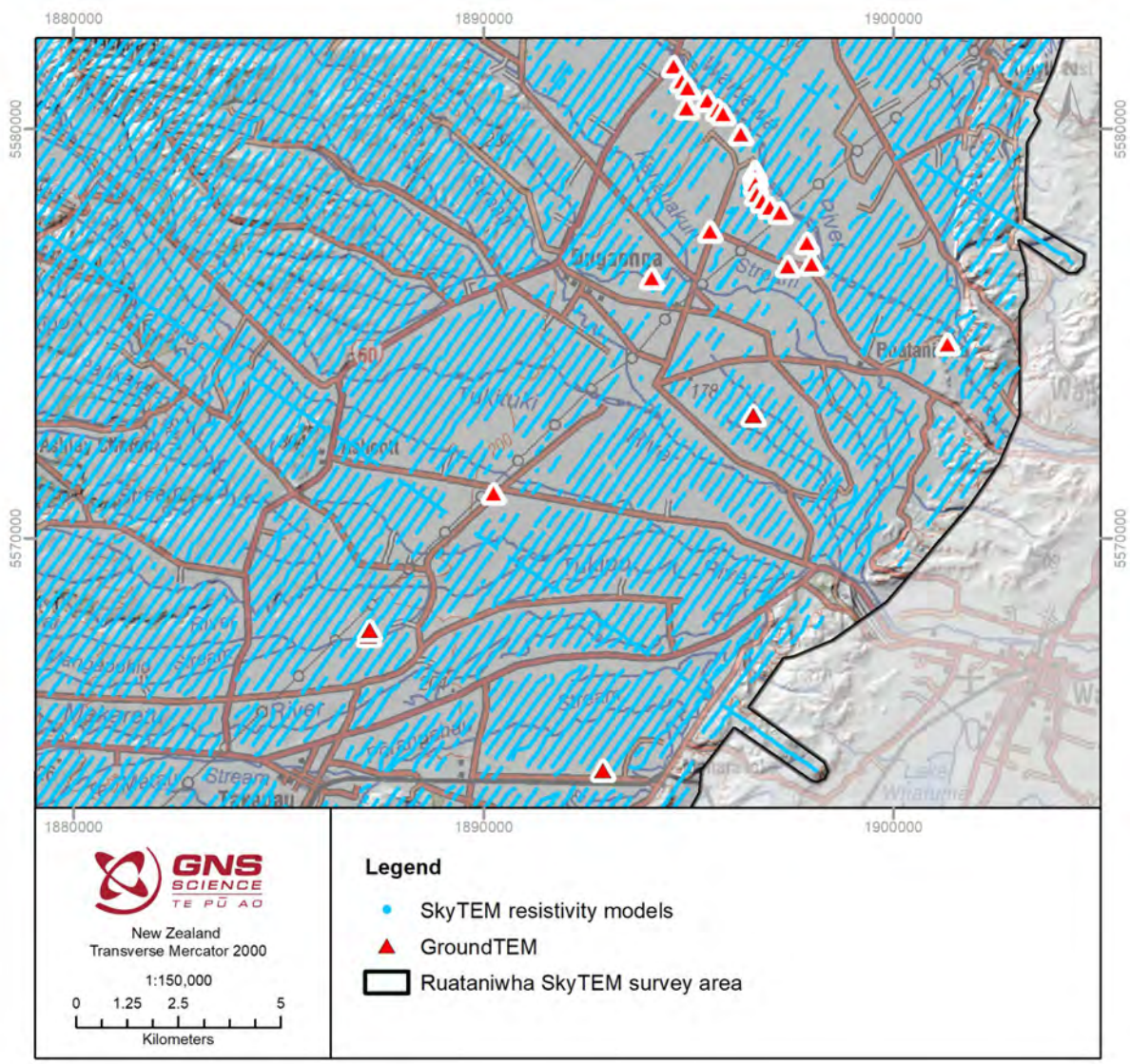

Figure 2.3 Ground-based resistivity data included within the combined resistivity dataset – some historic data is available within SkyTEM data gaps.

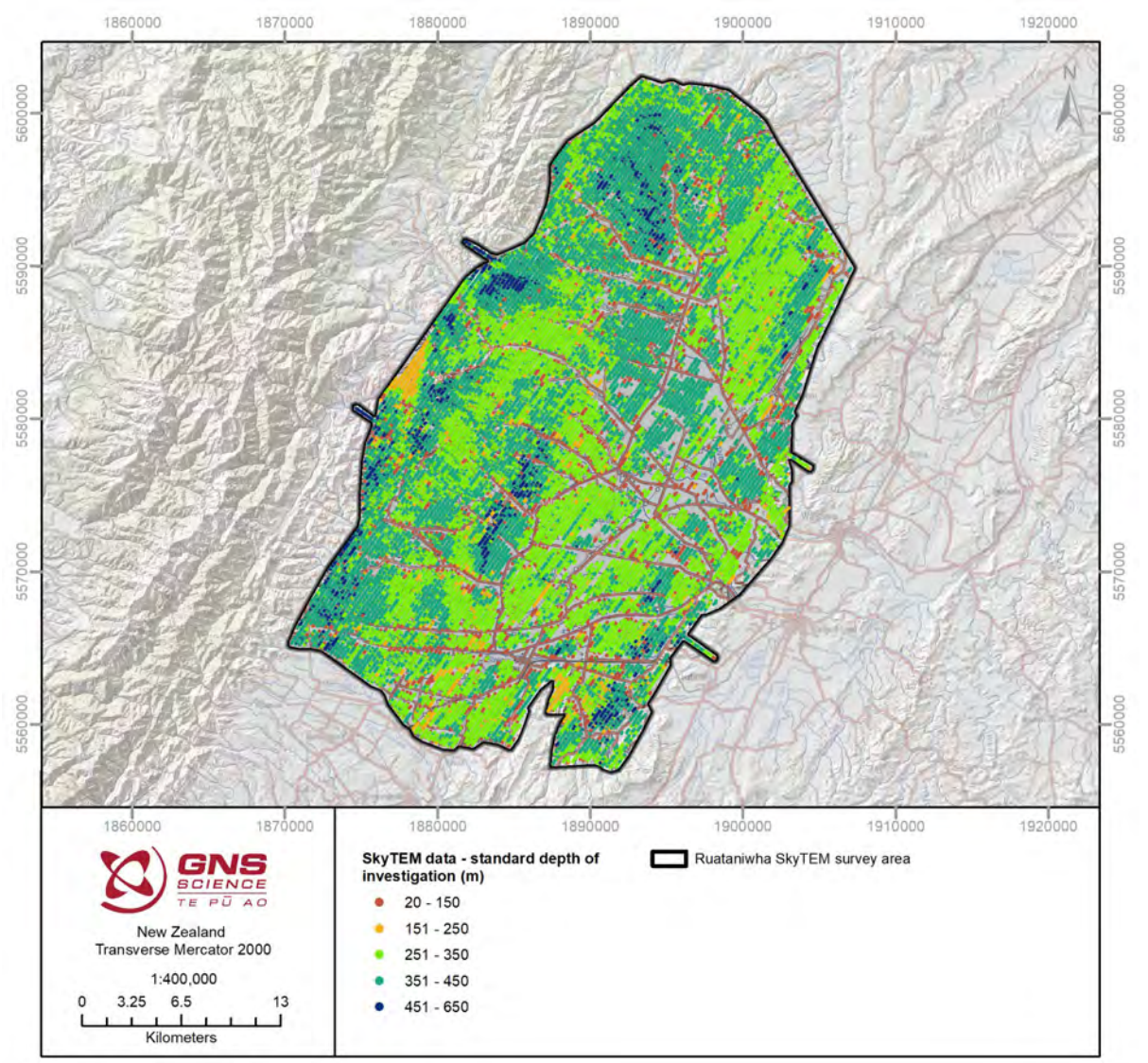

Figure 2.4 Standard depth of investigation for the SkyTEM-derived smooth resistivity models.

Table 2.1 Three-dimensional grid generated in Geoscene3D software (data mapped to cell nodes).

Corner Node Coordinates	Minimum	Maximum	Node Count	Width (m)	Node Spacing (m)
X	1870050	1907450	375	37,400	100
Y	5556950	5602550	457	45,600	100
Z	-348	650	500	998	2

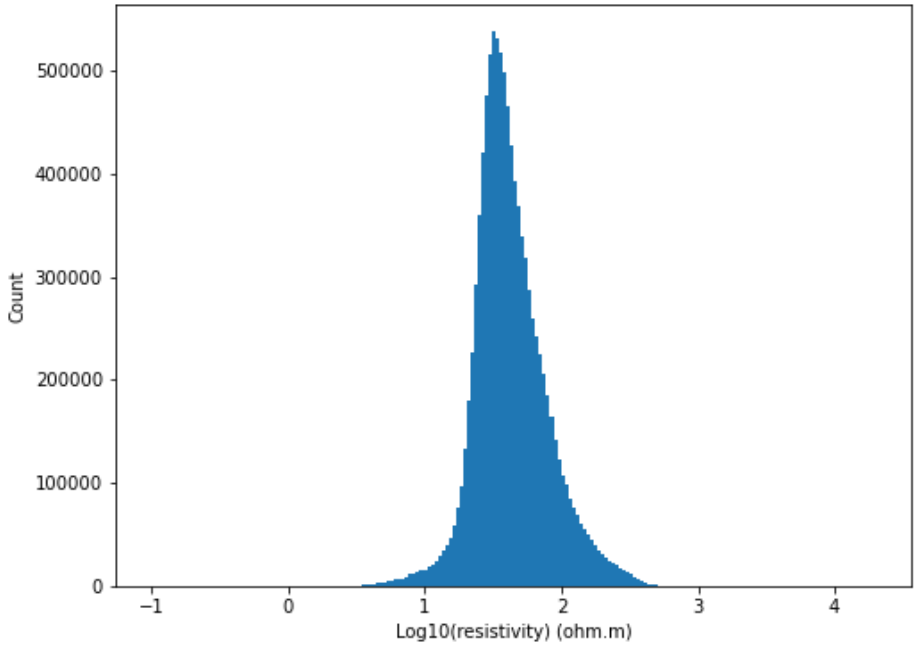

Figure 2.5 Histogram with 200 bins showing the $\log_{10}$(resistivity) values from the point dataset. The distribution approximates a Gaussian distribution.

2.1.2 Major Hydrogeological Unit (HU) Model

The manually delineated major hydrogeological unit (HU) surface from Sahoo et al. (2023) defining the top of basement was imported into Geoscene3D software (see Sahoo et al. [2023] for further details). This surface was developed to separate consolidated sediments (basement) and unconsolidated sediments within the Ruataniwha Plains model area (Sahoo et al. 2023), utilising the SkyTEM-derived resistivity models (Rawlinson et al. 2022).

Here, consolidated sediments are renamed to HU4 and unconsolidated sediments to HU2 (HU4 and HU2 are used for consistency with the Heretaunga Plains naming of basement and main aquifer unit; as such, HU1 and HU3 are not used in the major hydrogeological model [Rawlinson 2023]). To create a matching grid to the resistivity grid in Section 2.1.1, the 'Single Floating Point Type' 3D grid created in Section 2.1 was adjusted to a 'Word Discrete Value' type grid using the 'Convert Grid Value Type' in the Toolbox in Geoscene3D software, and two material categories were defined: HU2 and HU4. Geoscene3D stores information at cell node locations.

Hydrogeological units were assigned to the 3D grid (Table 2.2) using the manually delineated surfaces via the following steps:

- Assign null to all nodes.
- Assign HU4 to all nodes below HU4 top surface.
- Assign HU2 to all nodes above HU4 top surface and below DEM.
- Assign null to all nodes outside the Ruataniwha model boundary.

The gridded HU model was exported as a *.csv* file where values are mapped to cell nodes *x, y, z* and *HU*. Due to some discrepancies between cell resolution and surface resolutions, a few isolated single cells of HU2 were mapped at the surface within basement areas. To remove these, an additional Python script was utilised to remap cells classified as HU2 to HU4, where a single cell of HU2 was located at the maximum Z value and surrounded by HU4.

The exported hydrogeological unit and resistivity 3D grid files were combined into a single dataset (combined dataset), and to assist with later calculations, the elevation (Z) of the top model cell mapped with HU values was also determined (top_elev_HU). The dataset now has the columns *X, Y, Z, top_elev_HU, res, resvar* and *HU*. Because the HU model utilised a continuous surface throughout the entire model area, some locations that have gaps in the res model have values for the HU model (Table 2.2).

Table 2.2 Definition of the hydrogeological unit (HU) model.

Hydrogeological Unit (from Sahoo et al. [2023])	HU model	Description
HU2	2	Unconsolidated sediments
HU4	4	Basement unit

2.1.3 Hydrostratigraphic (HS) Model

Accumulated clay thickness (ACT) models were previously developed (Herpe and Rawlinson 2023) at locations of SkyTEM-derived resistivity models. The methodology combines information from lithological logs with the SkyTEM-derived resistivity models and allows for a variable spatial relationship between these using a translator function. Because the methodology utilised is only valid within unconsolidated sediments, the base was set using the manually delineated basement surface (Sahoo et al. 2023) with a 30 m buffer to account for layer clipping. The ACT modelling (Herpe and Rawlinson 2023) used the sharp resistivity model and so captures relevant information from that resistivity model for sharp boundary changes. This modelling resulted in Clay Fraction (CF) models and uses a binary assignment of lithological log information as part of the modelling (aquifer [low clay] or aquitard [high clay]).

Clustering of the ACT results was then used to define six categories of permeability (1–6; Figure 2.6; Table 2.3), where permeability is assumed to be primary controlled by clay content. Here, 6 is the most permeable material and 1 is the least permeable material. Clusters 4–6 correspond to <45% clay; clusters 1 and 2 correspond to >65% clay; and cluster 3 is a broad transitional group, ranging from 40–70% clay (Figure 2.6). Only 9% of the input data fall into the transitional cluster 3 group.

In contrast to the Heretaunga Plains HS work (Foged 2022), for the Ruataniwha Plains, 3D gridding and geostatistical simulations were not undertaken as part of this HSM. This was because of the following: (1) assessments of the Heretaunga HS results revealed limitations in the 10 m vertical resolution model utilised for the 500 geostatistical realisations (Rawlinson 2023); (2) Ruataniwha contains few SkyTEM data gaps (especially compared with the Heretaunga Plains); and (3) preliminary testing with the Heretaunga numerical groundwater model, determined that prior parameter conditioning (within current numerical modelling workflows) is likely best informed by the underlying ACT and cluster models at the locations of SkyTEM-derived resistivity models rather than the geostatistical realisations (Hemmings et al. [in prep]).

As such, CF and Cluster models are available as a point dataset at locations of SkyTEM-derived resistivity models. To map these point data to the combined model cell centres (Sections 2.1.1 and 2.1.2), a block model was created in Geoscience Analyst (Table 2.4). As per the identification of two anomalous points in Section 2.1.1, these points ([Easting, Northing] = [1899088.13, 5579937.00] and [Easting, Northing] = [1899068.00, 5579910.00]) were removed from the point dataset that had been vertically resampled to improve vertical resolution (from Herpe and Rawlinson 2023). This file was then imported as a point

dataset and transferred to the block model using the nearest neighbour function from Scipy.spatial.cKDTree (Maneewongvatana and Mount 2002; Virtanen et al. 2020). This method works for categorical (referenced) data as well as continuous data. All properties were transferred with a 500 m search radius. Here, *Cluster* is renamed to *HS_unclipped*. An additional nearest neighbour interpolation was undertaken with a 200 m search radius for *Cluster* only to ensure limited interpolation of values (for numerical modelling procedures being guided by the most certain information only). Here, *Cluster* retains the name *Cluster*. This block model was exported as a *.csv* file with columns *X, Y, Z, CF, CF_STD, Cluster, Silhouette_Index and HS_unclipped*, where *X, Y, Z* corresponds to the same cell centres as the combined dataset. Here, *CF_STD* is the standard deviation of the *CF* model and provides a measure of uncertainty for *CF,* while *Silhouette_Index* provides a measure of uncertainty for *Cluster* and *HS_unclipped* (see Figure 2.6). The silhouette index is a measure of how similar an object is to its own cluster (cohesion) compared with other clusters (separation). The mean silhouette index for the dataset is 0.55, and above this value cluster values are considered well-determined.

This dataset was joined at X, Y and Z locations to the combined dataset. Because the ACT methodology is only valid within the unconsolidated sediments, an additional join was made to the combined dataset where HU is not basement (HU<4) to create the HS model. The combined dataset now has columns *X, Y, Z, top_elev_HU, res, resvar, HU, CF, CF_STD, Cluster, Silhouette_Index, HS_unclipped* and *HS*.

Table 2.3 Hydrostratigraphic (HS) model. Permeability is estimated from Figure 2.6.

HS Model	Permeability	Percentage of HS Cells (%)
6	High (<10% clay)	16
5	High (<20% clay)	22
4	High to medium (10–45% clay)	8
3	Medium to low (40–70% clay)	9
2	Low (65–90% clay)	13
1	Low (>70% clay)	32

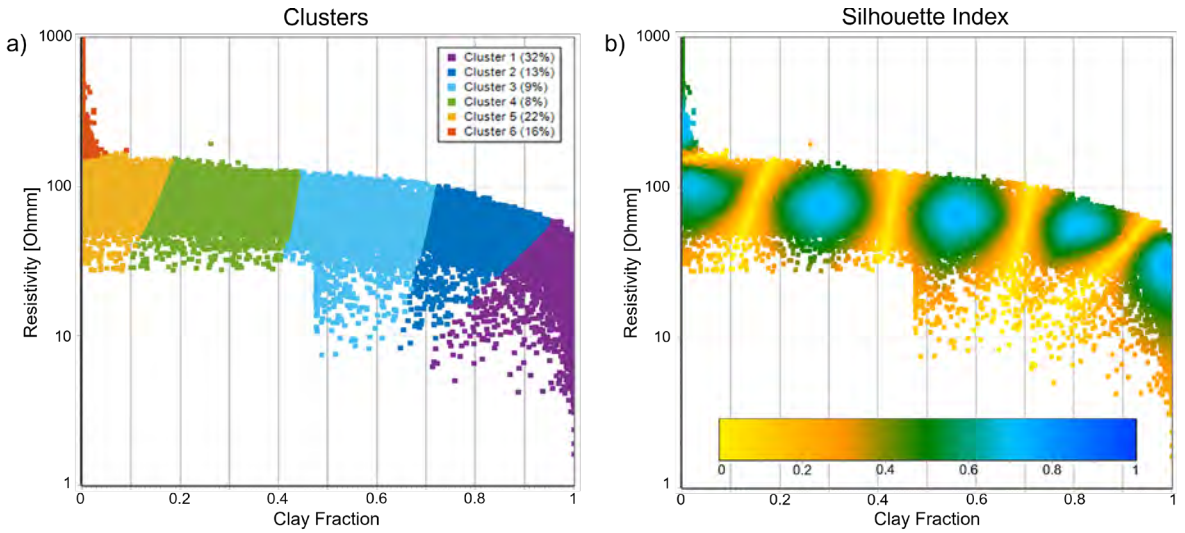

Figure 2.6 Six accumulated clay thickness (ACT) clusters. (a) Input clay fraction (CF) and resistivity data (x,y axis) and the resulting cluster group (dot colour); (b) Corresponding silhouette index. The mean silhouette index is 0.55, and above this value clusters are considered well-determined. Figure from Herpe and Rawlinson (2023).

Table 2.4 Three-dimensional grid generated in Geoscience Analyst software (data mapped to cell centres).

Corner Node Coordinates	Minimum	Maximum	Number of Cells	Grid Size (m)	Cell Size (m)
X	1870000	1907500	375	37,500	100
Y	5556900	5602600	457	45,700	100
Z	-349	651	500	1000	2

2.1.4 Resistivity Facies (facies) Model

As significant changes within resistivity are best assessed on a logarithmic scale, resistivity facies were defined by separating the res model into 14 resistivity facies classes (facies) uniformly separated on a log scale (Table 2.5; for example, Minsley et al. [2021]). These facies classes group materials that are expected to have similar hydrologic and geologic properties based on their resistivity, to assist with easier discrimination of significant variability and similarity.

Log_{10}-transformed res model values were classified into uniform bins with a width of 0.15 between 0.9 and 2.7 (Table 2.5). These values were chosen based on detailed assessments of resistivity values against relevant datasets described within Tschritter et al. (2022), such as lithological logs, as well as assessments provided in Kellett et al. (2023), Sahoo et al. (2023) and Herpe and Rawlinson (2023). The intervals are the same as those used within Rawlinson (2023) for the Heretaunga Plains area.

Resistivity values in the *res* column (interpolated resistivity model from Section 2.1.1) were converted to resistivity facies classes using the combined dataset, which now has columns *X, Y, Z, top_elev_HU, res, resvar, HU, CF, CF_STD, Cluster, Silhouette_Index, HS_unclipped, HS* and *facies*.

Table 2.5 Resistivity facies (facies) model definition, using resistivity values within the res model.

Facies	Lower-Bound Log_{10}(res)	Upper-Bound Log_{10}(res)	Lower-Bound res model (ohm.m)	Upper-Bound res model (ohm.m)
1	NA	0.90	NA	8
2	0.90	1.05	8	11
3	1.05	1.20	11	16
4	1.20	1.35	16	22
5	1.35	1.50	22	32
6	1.50	1.65	32	45
7	1.65	1.80	45	63
8	1.80	1.95	63	89
9	1.95	2.10	89	126
10	2.10	2.25	126	178
11	2.25	2.40	178	251
12	2.40	2.55	251	355
13	2.55	2.70	355	501
14	2.70	NA	501	NA

2.1.5 Aquifer Potential (AP) Model

An Aquifer Potential (AP) model was developed to separate the facies model into consolidated and unconsolidated sediments, whilst providing an indicator of the likelihood of each model cell to host aquifer-bearing material. AP classes were defined by establishing rules within the major hydrogeological units as to how each resistivity facies class maps to aquifer potential. The naming 'aquifer potential' refers to the likelihood that a particular cell may host aquifer-bearing material.

The primary mapping of facies to aquifer potential was undertaken by first defining resistivity thresholds upon which low, medium and high aquifer potential were defined. This separates the dataset into a simplified text category with six classes 'aq', mapping values to consolidated low, medium and high aquifer potential and unconsolidated low, medium and high aquifer potential. Threshold values were chosen based on detailed assessments of resistivity against relevant datasets described within Tschritter et al. (2022), such as lithological logs and QMAP main rock type, as well as assessments provided in Kellett et al. (2023), Sahoo et al. (2023) and Herpe and Rawlinson (2023).

The unconsolidated sediments (HU2) were observed to follow a linear relationship between resistivity and aquifer potential (as expected). Unconsolidated medium and high aquifer potential thresholds were set at 45 and 89 ohm.m, respectively, which coincide with the facies upper boundaries of classes 6 and 8. Therefore, for unconsolidated sediments, facies classes 1–6 are defined as low aquifer potential, classes 7–8 are defined as medium aquifer potential, and classes 9–14 are classified as high aquifer potential. Due to the linear relationship observed, aquifer potential in the unconsolidated sediments is expected to gradually increase as the facies classes increase in value. To develop unique aquifer potential classes, these 14 facies classes within unconsolidated sediments (HU2) were mapped to the aquifer potential numbers 15–28 (Table 2.6).

For consolidated sediments (HU4; corresponding in this area to mudstone/siltstone, sandstone and limestone), the relationship is not completely linear. Limestone is assumed to have a mostly linear relationship with resistivity, with more massive (consolidated) limestone having higher resistivity and more permeable limestone having lower resistivity (e.g. Figure 1.2). However, there is a complication in that lower resistivity corresponds to less consolidated and/or silt, while higher resistivity corresponds to more consolidated and/or less silt, as well as to outcropping limestone. Mudstone/siltstone corresponds to low permeability and to low resistivity in the area (see below). Sandstone corresponds to medium permeability and medium resistivity in the area (see below). Due to this relationship, three threshold values were required – two threshold values for splitting into medium and high potential and an additional threshold at a high resistivity value for splitting into low potential again. Thresholds for splitting into low, medium and high aquifer potential were defined at values of 22 and 45 ohm.m, and then an upper threshold of 355 ohm.m was selected above which limestone becomes too tight and aquifer potential drops. Therefore, for consolidated sediments, facies classes 1–4 and 13–14 are defined as low aquifer potential, classes 5–6 are defined as medium aquifer potential and classes 7–12 are classified as high aquifer potential. These were mapped in order from low to high to the aquifer potential numbers 1–14 (Table 2.6).

These medium and high consolidated threshold values are consistent with the values for limestone utilised within the Poukawa SkyTEM interpretation report (Rawlinson et al. [in prep]), which had a higher volume of limestone material available for analysis, as well as the values utilised within the Heretaunga SkyTEM interpretation report (Rawlinson 2023). However, the third (highest) threshold value is set higher than in Rawlinson (2023) and

Rawlinson et al. (in prep) based on an assessment of screened limestone bores in the eastern ranges. These threshold values also considered the comparison of available mudstone and sandstone information against resistivity values in the area, with low aquifer potential being consistent with containing <10% limestone and sandstone, and high aquifer potential being consistent with containing <10% mudstone.

Using the above approach, aquifer potential classes 1–28 were defined using the combined columns *facies* and *HU*. This calculation was made on the combined dataset, which now has columns *X, Y, Z, top_elev_HU, res, resvar, HU, CF, CF_STD, Cluster, Silhouette_Index, HS_unclipped, HS, facies*, *AP* and *aq*.

Table 2.6 Aquifer Potential (AP) model definition, which uses the defined resistivity facies (facies) classes from Table 2.5 and the major hydrogeological unit (HU) classes from Table 2.2. Also defined is a simplified aquifer potential model with only six classes 'aq' and 'aq name'.

AP	HU	Facies	aq	aq name	Lower-Bound res (ohm.m)	Upper-Bound res (ohm.m)
1	4	1	cl	Consolidated-low	NA	8
2	4	2	cl	Consolidated-low	8	11
3	4	3	cl	Consolidated-low	11	16
4	4	4	cl	Consolidated-low	16	22
5	4	13	cl	Consolidated-low	355	501
6	4	14	cl	Consolidated-low	501	5000
7	4	5	cm	Consolidated-med	22	32
8	4	6	cm	Consolidated-med	32	45
9	4	7	ch	Consolidated-high	45	63
10	4	8	ch	Consolidated-high	63	89
11	4	9	ch	Consolidated-high	89	126
12	4	10	ch	Consolidated-high	126	178
13	4	11	ch	Consolidated-high	178	251
14	4	12	ch	Consolidated-high	251	355
15	2	1	ul	Unconsolidated-low	1	8
16	2	2	ul	Unconsolidated-low	8	11
17	2	3	ul	Unconsolidated-low	11	16
18	2	4	ul	Unconsolidated-low	16	22
19	2	5	ul	Unconsolidated-low	22	32
20	2	6	ul	Unconsolidated-low	32	45
21	2	7	um	Unconsolidated-med	45	63
22	2	8	um	Unconsolidated-med	63	89
23	2	9	uh	Unconsolidated-high	89	126
24	2	10	uh	Unconsolidated-high	126	178
25	2	11	uh	Unconsolidated-high	178	251
26	2	12	uh	Unconsolidated-high	251	355
27	2	13	uh	Unconsolidated-high	355	501
28	2	14	uh	Unconsolidated-high	501	NA

2.1.6 Coarse-Fraction Classification (CC) Model

A coarse-fraction classification (CC) model was developed for the following two reasons:

1. **Value of a continuous coarse-fraction classification model to compare to hydraulic conductivity values.** For supporting translations of hydrogeological interpretations of SkyTEM data to hydraulic conductivity suitable for numerical groundwater flow modelling, Rawlinson (2023) demonstrated the value of being able to map expert- and flow model-informed hydraulic conductivity values against a continuous coarse-fraction classification model.
2. **Different spatial-coverage limitations of the HS and AP models.** The HS model utilises borehole information and a spatially varying function that maps the relationship between resistivity and permeability (clay-fraction); however, it is only valid within the unconsolidated sediments. The AP model is a more simplistic model that does not provide a spatially varying translator function; however, it is also able to provide more information on consolidated sediments.

   Numerical flow models may require information to be provided even within basement areas of the model to, for example, better consider flux from limestone. As the HS model does not provide information on the consolidated geology, while the AP model does, a combination between the AP and HS models is required to provide best information to numerical flow models.

To combine the strengths of the AP and HS models, a final dataset was created – the CC model – that combines these models.

Contrary to the HS model developed for the Heretaunga Plains, which had a vertical resolution of 10 m (Section 2.1.3; Foged 2022; Rawlinson 2023), the HS model developed for Ruataniwha Plains largely retains the original resolution of the SkyTEM dataset (shallowest layer has ~2 m vertical resolution; Herpe and Rawlinson 2023). Upon manual inspection of available lithological logs versus the AP and HS models, although some differences are apparent, there are no obvious areas or lithological log types where one model out-performs the other. Additionally, although the majority of pumping tests have been performed in AP >=20 (see Section 2.1.7), most hydraulic conductivity values estimated in the Ruataniwha Plains tend to be low (<200 m/day; Section 2.1.7) and all are less than 1000 m/day. As such, in contrast to the Heretaunga Plains (Rawlinson 2023), there is no distinct AP/HS combination that corresponds to increased permeability or that requires up-weighting in either model.

Due to the above assessment, within the unconsolidated sediments (HU<4), the CC model was calculated directly from the CF model.

$$CC = 1 - CF \qquad \text{Equation 2.1}$$

However, due to numerical limitations utilising a model containing zero values, any zero values were remapped to CC = 0.002. This value was selected because the smallest value other than zero was CC = 0.01, and this also enables mapping of the consolidated sediments into CC values between 0 and 0.002. Basement values from the AP model (1–14) were normalised by 10000 and mapped directly into the CC model as a discrete range of classes 0.0001–0.0014. Where basement was defined (HU4) and there was no AP model, but the *HS_unclipped* model existed, CC was set to 0.0001, 0.0003, 0.0006, 0.0009, 0.0011 and 0.0014 for *HS_unclipped* = 1–6. Where basement was defined (HU = 4), but the AP or *HS_unclipped* models were not present, CC was set to 0.0001.

Within the CC model, values >0.5 are considered to be the equivalent of >50% coarse material and defined here as an aquifer, while values <=0.5 are considered to be the equivalent of <=50% coarse material and defined here as an aquitard. This assumption of correspondence to coarse fraction was checked against lab-based coarse-fraction estimates from seven different boreholes (3DAMP_Well1, 3DAMP_Well3, and five new SOE bores; Tschritter et al. [2022]). From these boreholes, the sample resistivity was checked against grain size, confirming the expected trend of decreasing resistivity with decreasing grain size (Figure 2.7). Here, all samples with >0.5 fine-grained fraction (clay and silt) have resistivity values less than 30 ohm.m. Figure 2.8 displays a comparison of CC model values against these lab-based coarse-fraction estimates. Considering the resolution of the 3D model grid, before this comparison, the dataset was cleaned to remove grain size measurements corresponding to very short logged intervals surrounded by larger volumes of material with different properties. Additionally, as there are very fine sands in Ruataniwha Plains with low permeability, the grain-size analyses displayed in Figure 2.8 were calculated based on all material with grain sizes corresponding to medium sands or greater. After these corrections for scale/volume-equivalencies, the CC model successfully identifies material as either aquifer or aquitard (Figure 2.8; taking 50% coarse material as the threshold value between aquifer and aquitard). However, due to the binary nature of the utilised CF model (designed to define either aquifer or aquitard), a large number of the CC model values map close to 0 or 1.

The CC model calculation was made on the combined dataset, which now has columns *X, Y, Z, top_elev_HU, res, resvar, HU, CF, CF_STD, Cluster, Silhouette_Index, HS_unclipped, HS, facies*, *AP, aq* and *CC*.

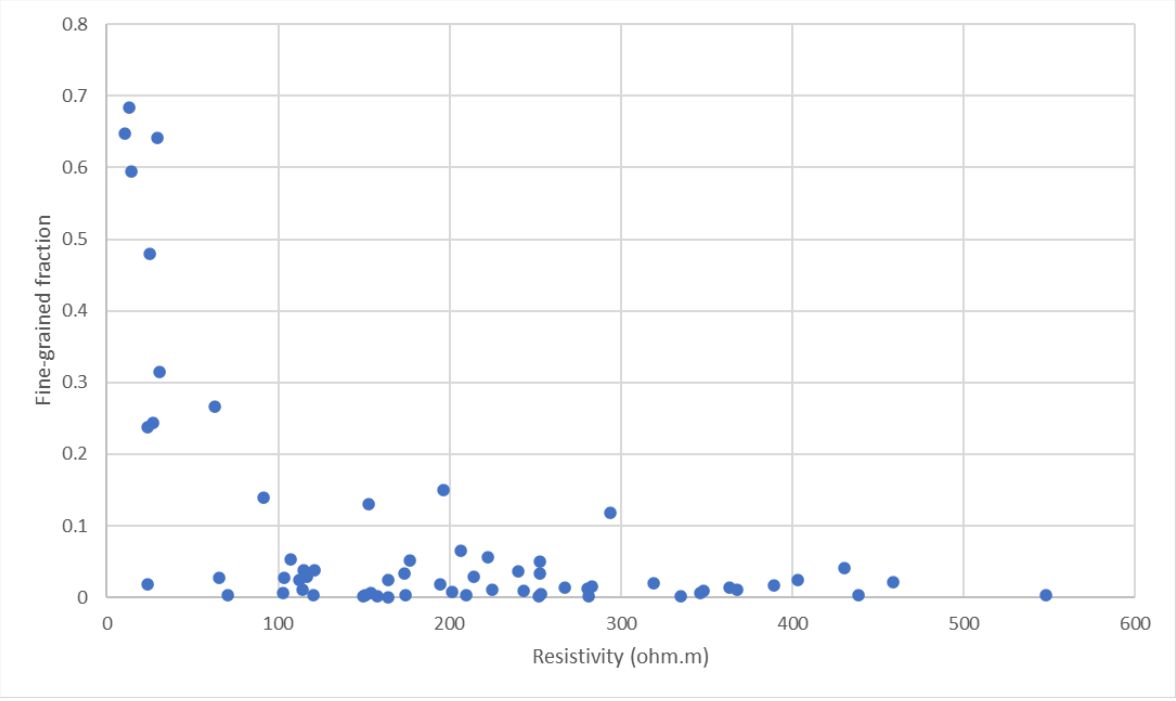

Figure 2.7 Fine-grained fraction of material samples from lab-based grain-size analysis versus resistivity of samples from resistivity cells. All samples with >0.5 fine-grained fraction have resistivity values less than 30 ohm.m. Data is from seven different boreholes (3DAMP_Well1, 3DAMP_Well3, and five new SOE bores; Tschritter et al. 2022). Fine-grained material corresponds to clay and silt.

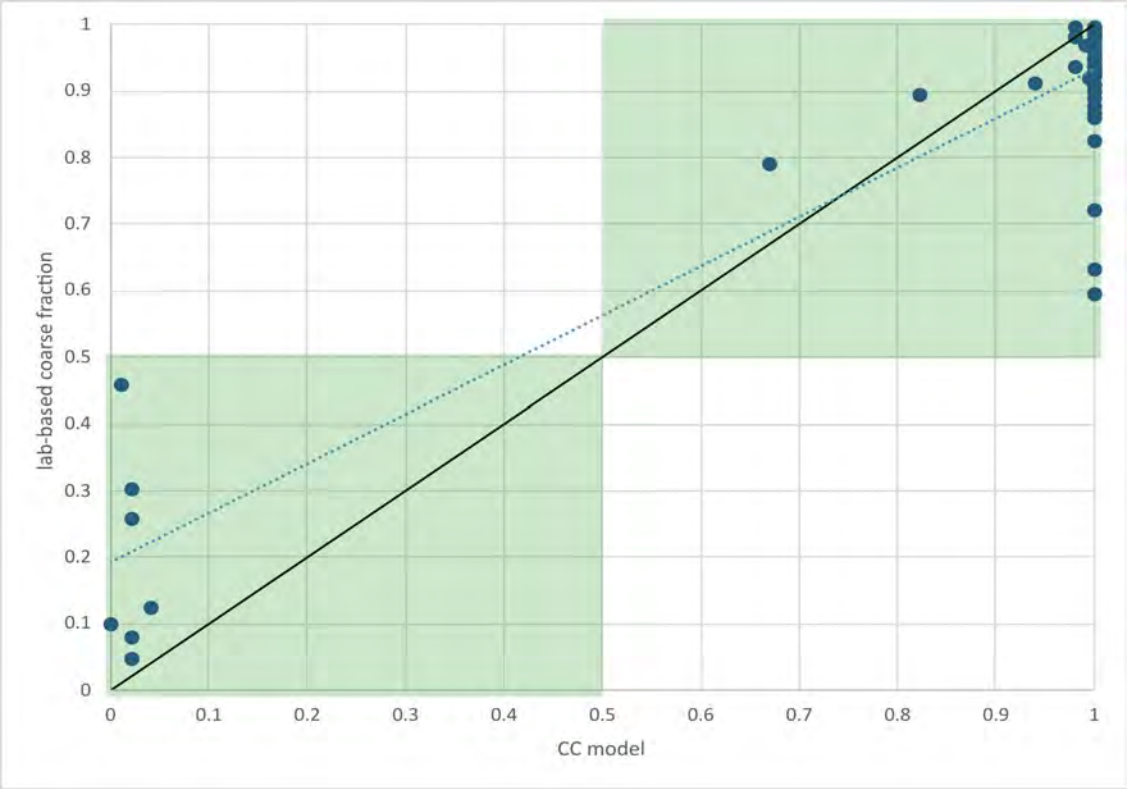

Figure 2.8 Lab-based coarse fraction estimates are based on grain sizes from medium sand or greater. Green boxes define where the CC model matches lab-based coarse fraction estimates in terms of classification into aquifer or aquitard using the 0.5 threshold. Black line shows one-to-one. Blue dotted line shows linear trend from data points.

2.1.7 Horizontal Hydraulic Conductivity (KH)

In this section, the relationship between the previously developed 3D models and estimates of horizontal hydraulic conductivity K_H from aquifer tests is explored.

The link between geoelectric properties and hydraulic conductivity is complex, as both the porosity and geometry of pore spaces cannot be uniquely determined using electrical resistivity. A large number of studies have been performed, with seemingly contradictory empirical relationships between resistivity and hydraulic conductivity being determined: both direct and inverse relationships (e.g. Niwas and Celik [2012] and references therein). This is because the Archie's law assumption that all electrical conduction is through fluid-filled pore space is erroneous. In support of this, it has been theoretically derived by Purvance and Andricevic (2000) that an inverse relationship is obtained when interconnected pore volumes dominate electrical current flow and a direct relationship obtained when the interconnected pore surface areas dominate electrical current flow (Slater 2007). This results in the commonly empirically determined linear log-log relationship between horizontal hydraulic conductivity K_H and resistivity ρ:

$$K_H = b\rho^c \qquad \text{Equation 2.2}$$

or

$$log_{10} K_H = c\, log_{10}\, \rho + d \qquad \text{Equation 2.3}$$

where the constant values *b*, *c* and *d* are empirically determined. When pore volume conduction dominates, *c* is negative, while when pore surface area conduction dominates, *c* is positive (Purvance and Andricevic 2000). To satisfy theoretical constraints, there must only

be small variations in water conductivity, anisotropy (of pore size distributions impacting hydraulic conductivity), cementation and porosity over the volume investigated (Purvance and Andricevic 2000). Hydraulic data must also be scaled so that equal-scale hydraulic conductivity and electrical conductivity values are being compared (Purvance and Andricevic 2000). The applicability of this correlation will therefore depend on the particular properties of the aquifer under investigation.

Pore surface area conduction dominates in freshwater-clay environments, such as the Ruataniwha Plains, due to the increased resistivity of freshwater (compared with saline water) and the fine-grained nature of clay increasing the internal surface area (Purvance and Andricevic 2000). This results in an increase in electrical resistivity associated with an increase in permeability.

As Figure 2.9 displays, there is substantial variance that has previously been found through different empirical estimates from studies of different aquifers. As discussed by Purvance and Andricevic (2000), these large variances are likely to do with the local depositional environment and anisotropy of the aquifer properties. A brief exploration into this correlation in the Ruataniwha Plains was previously performed by Meilhac et al. (2009), where an empirical relationship was derived between resistivity from NanoTEM measurements and hydraulic conductivity estimates from slug tests (Figure 2.10), and used to construct a hydraulic conductivity profile along the Waipawa River in the Ruataniwha Plains.

In many sedimentary and glacial deposition environments, clay content can be considered as inversely proportional to hydraulic conductivity. Previous studies have also empirically determined a relationship between the fraction of coarse material (F_c) and horizontal hydraulic conductivity K_H, e.g. this linear equation from Faunt (2009): $K_H = F_c K_c + F_f K_f$. Here, F_f is defined as $1 - F_c$, K_c is set as the maximum hydraulic conductivity for a cell composed of 100% coarse material, and K_f is set as the minimum hydraulic conductivity for a cell composed of 100% firm clay.

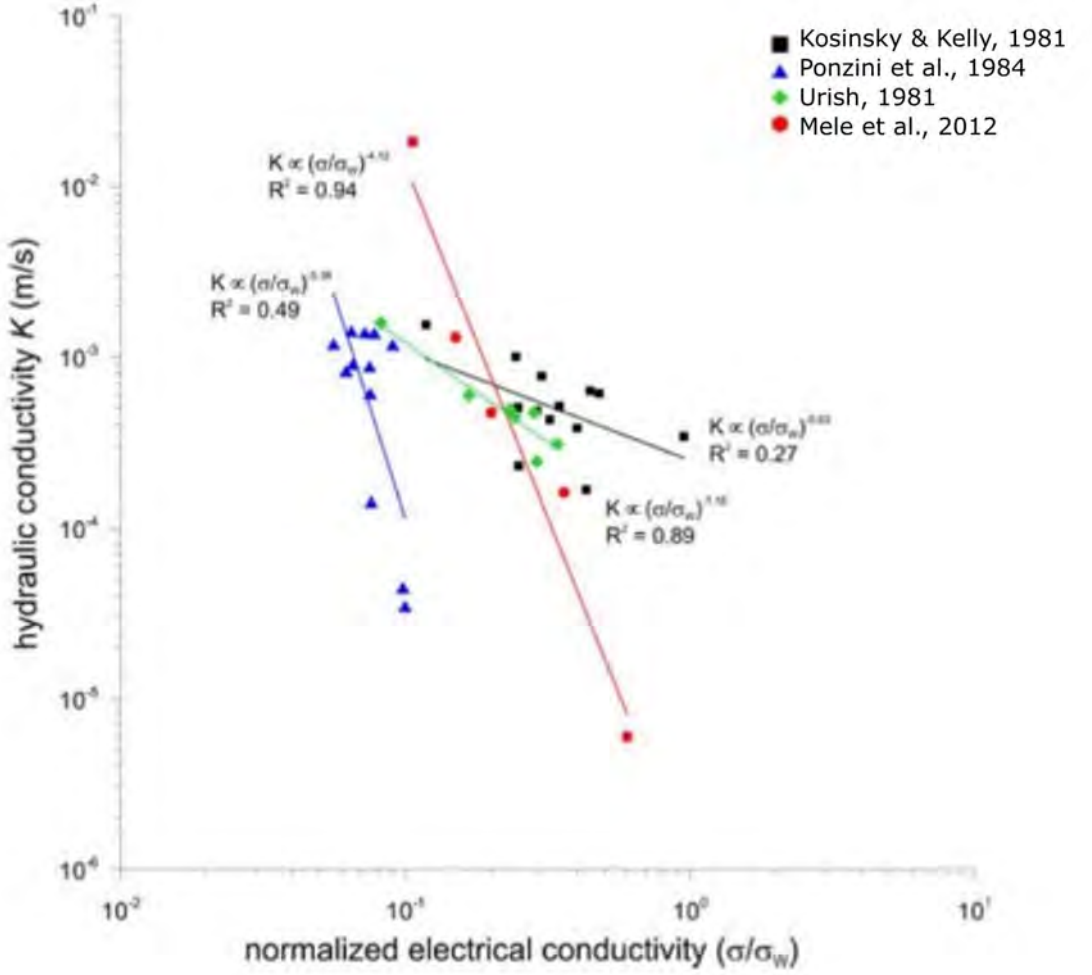

Figure 2.9 Correlation between average hydraulic conductivity (K) and normalised electrical conductivity (inverse of resistivity) of freshwater-saturated hydrofacies (σ_w: average electrical conductivity of pore water) and comparison with negative field-scale correlations cited in the literature (Kosinski and Kelly 1981; Ponzini et al. 1984; Urish 1981). Figure and caption adapted from Mele et al. (2012). The relationships shown are equivalent to an increase in electrical resistivity corresponding to an increase in permeability. Normalisation was performed for a more direct comparison between the different study areas.

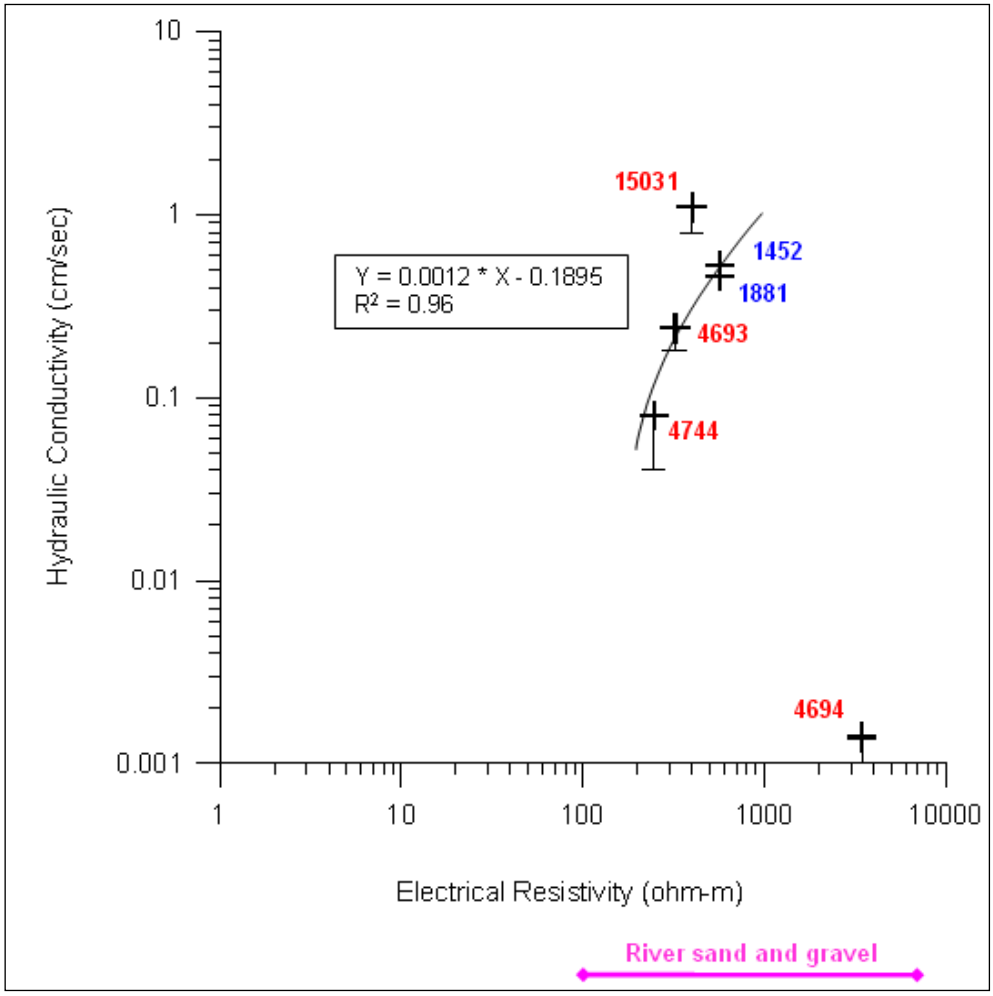

Figure 2.10 Correlation between hydraulic conductivity obtained from aquifer tests and electrical resistivity obtained from NanoTEM in the Ruataniwha Plains, Hawke's Bay. Figure from Meilhac et al. (2009).

2.1.7.1 Hydraulic Conductivity Dataset

The previously compiled hydraulic conductivity (K_H) dataset for the Ruataniwha Plains from Tschritter et al. (2022) was utilised for this assessment. To ensure all hydraulic conductivity values were consistently obtained, new K_H estimates were calculated from available transmissivity values. Where transmissivity estimates were not available, the existing K_H estimates were utilised.

The identified screen-lengths in this dataset were cross-checked against the water supply intervals defined by Tschritter et al. (2022) and any discrepancies between the datasets cross-checked against the lithological log to assist with appropriate value selection. The screen-lengths in the Tschritter et al. (2022) K_H dataset were confirmed as the best dataset. Estimates of hydraulic conductivity were made by dividing the transmissivity obtained from the pumping tests by the screen length with an additional 4 m added – corresponding to an additional 2 m above and 2 m below the top and bottom of the screen. This is where the influence of pumping is assumed to be most significant (extrapolating from isolines for pumping shown in Bouwer and Rice [1976]; Perwick and Woodhouse [2014]; and Moore [2023]).

Figure 2.11 shows the resulting new K_H estimates. The dataset includes a lot of low K_H estimates and there is no clear pattern discernible. Of note for assessing the validity of using this pumping dataset as the primary source to compare to the 3D models is that the dataset source is, by its nature, biased toward higher K_H values. Slug and pumping tests are difficult

to obtain in low permeability sediments due to the long wait times for the water levels to return to equilibrium. Additionally, pumping tests are usually only performed within sediments with enough permeability that they are desirable to be used for a water supply. Some low permeability sediments were selected for slug testing as part of the 3DAMP drilling programme at 3DAMP_Well1 and 3DAMP_Well3 (Lawrence et al. 2022a, 2022b); however, these values compose a small percentage of the dataset. Information on expected K_H values for lower permeability unconsolidated sediments from the literature provide $K_H = 10^{-4} – 10^{-7}$ m/day for clay, $K_H = 1 – 10^{-3}$ for silt and $K_H = 10^{-1} – 10$ m/day for silty sand (Heath 1983).

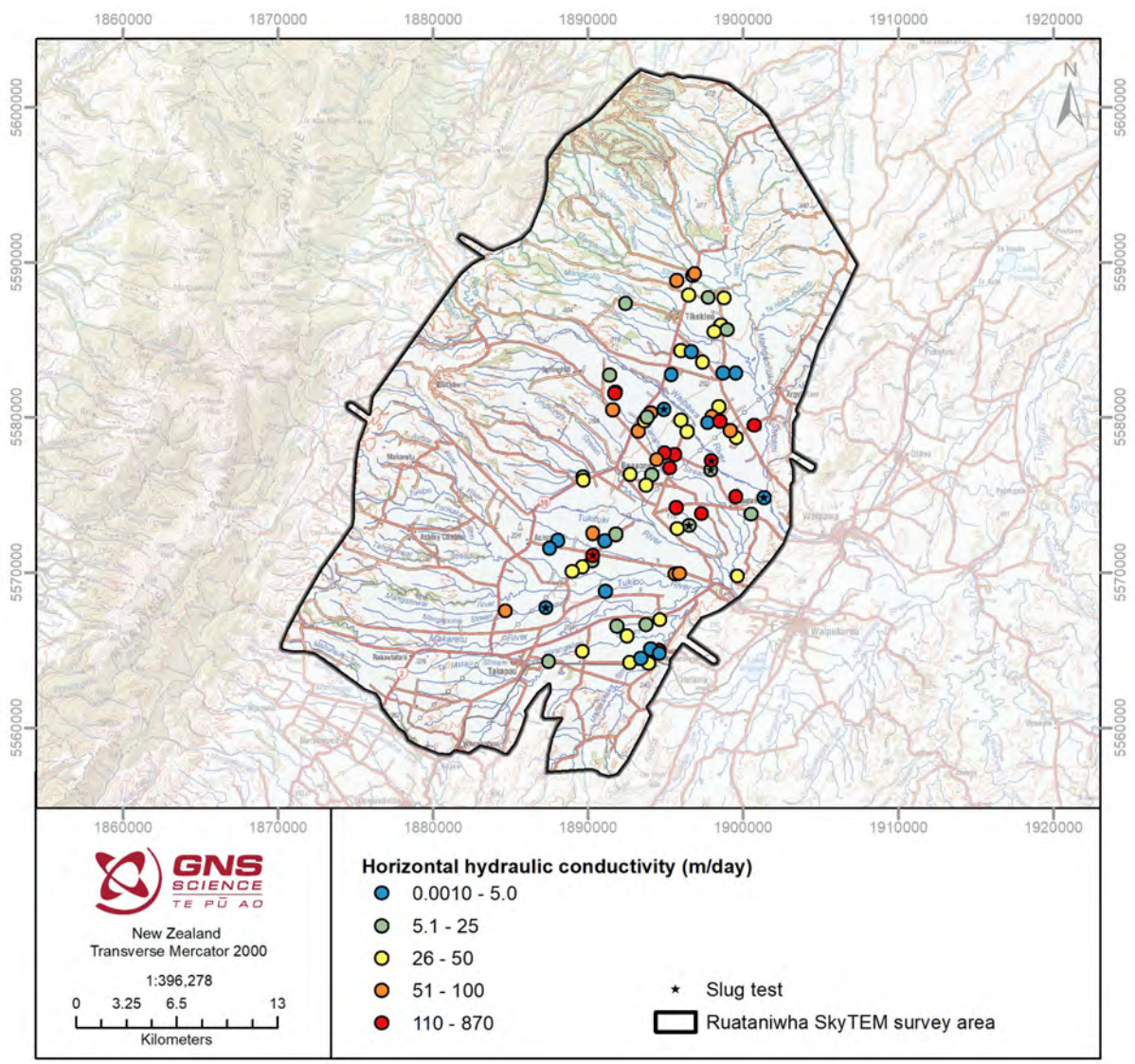

Figure 2.11 Quality-checked and corrected horizontal hydraulic conductivity (K_H) values used for comparison with the SkyTEM-derived 3D models.

2.1.7.2 Comparison of K_H Dataset to 3D Models

Due to significant differences in the volumes of material sampled, slug tests were not compared to the 3D models. Additionally, only unconsolidated material was compared to the 3D models, so pumping tests noted as being within limestone, sandstone or mudstone were not included within the analysis. 3D model data were selected within the same horizontal cell as the pumping bore, and vertical cells were selected covering the screen interval, +2 m above the screen and -2 m below the screen (the same interval considered most influential during pumping and used

for the transmissivity to K_H conversion in Section 2.1.7.1). As the 3D models have a 2 m vertical cell resolution, multiple cells with potentially different model values were thus selected. From these selected cells, for each different 3D model, the geometric mean was calculated.

Graphs showing the results of this comparison are shown below for the res model (Figure 2.12), the AP model (Figure 2.13), the HS model (Figure 2.14) and the CC model (Figure 2.15). For the continuous res and CC models, linear regression equations were determined and the associated residual standard error (RSE) calculated.

As expected for the Ruataniwha Plains aquifer environment, direct (rather than inverse) equations were empirically determined – where an increase in resistivity corresponds to an increase in permeability and where clay content is inversely proportional to hydraulic conductivity:

$$Log_{10}(K_H) = 0.8027 Log_{10}(res) - 0.0322 \qquad (RSE = 0.48) \qquad \text{Equation 2.4}$$

$$Log_{10}(K_H) = 0.429 CC + 1.2285 \qquad (RSE = 0.47) \qquad \text{Equation 2.5}$$

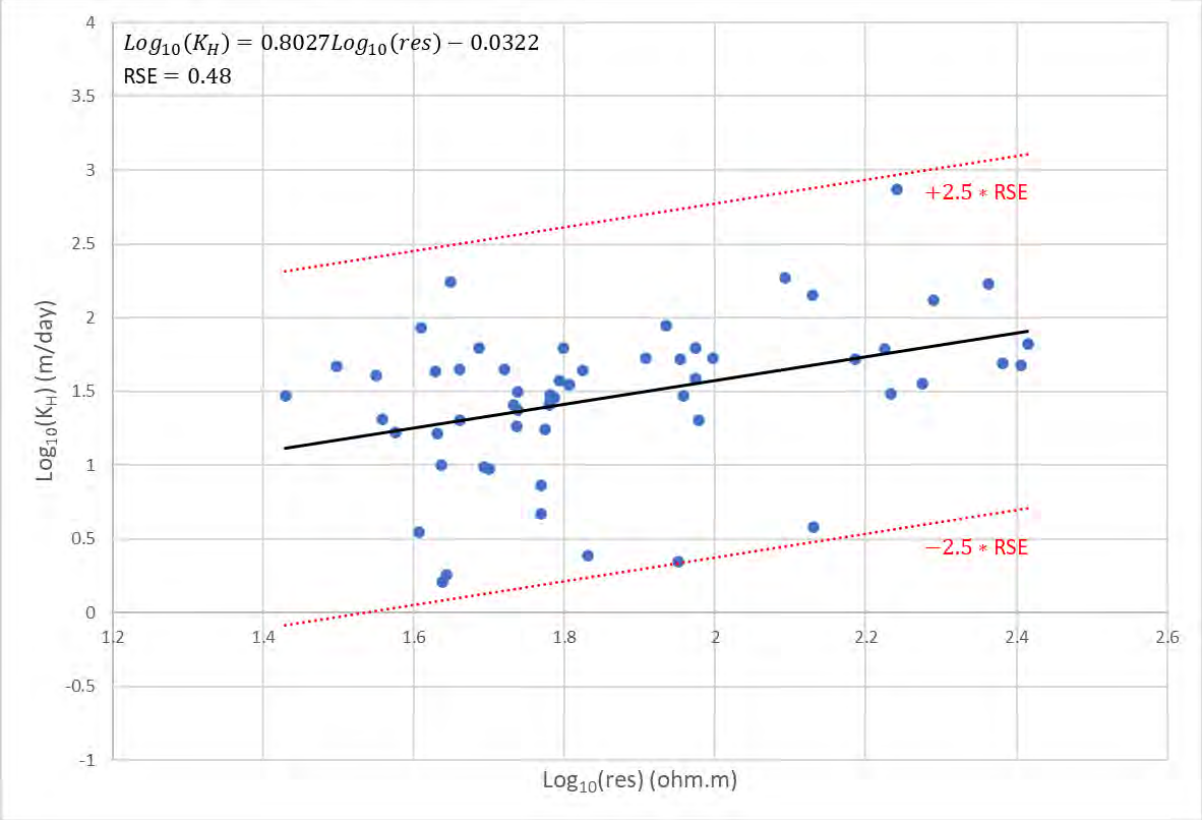

Figure 2.12 Horizontal hydraulic conductivity (K_H) versus res model linear regression equation, as well as +/-2.5*RSE. RSE is an estimate of the variance of the error term for the equation fit to data, and 95% of values are expected to be found within 2*RSE. Blue points are the estimates of K_H made from pumping test data (Section 2.1.7.1).

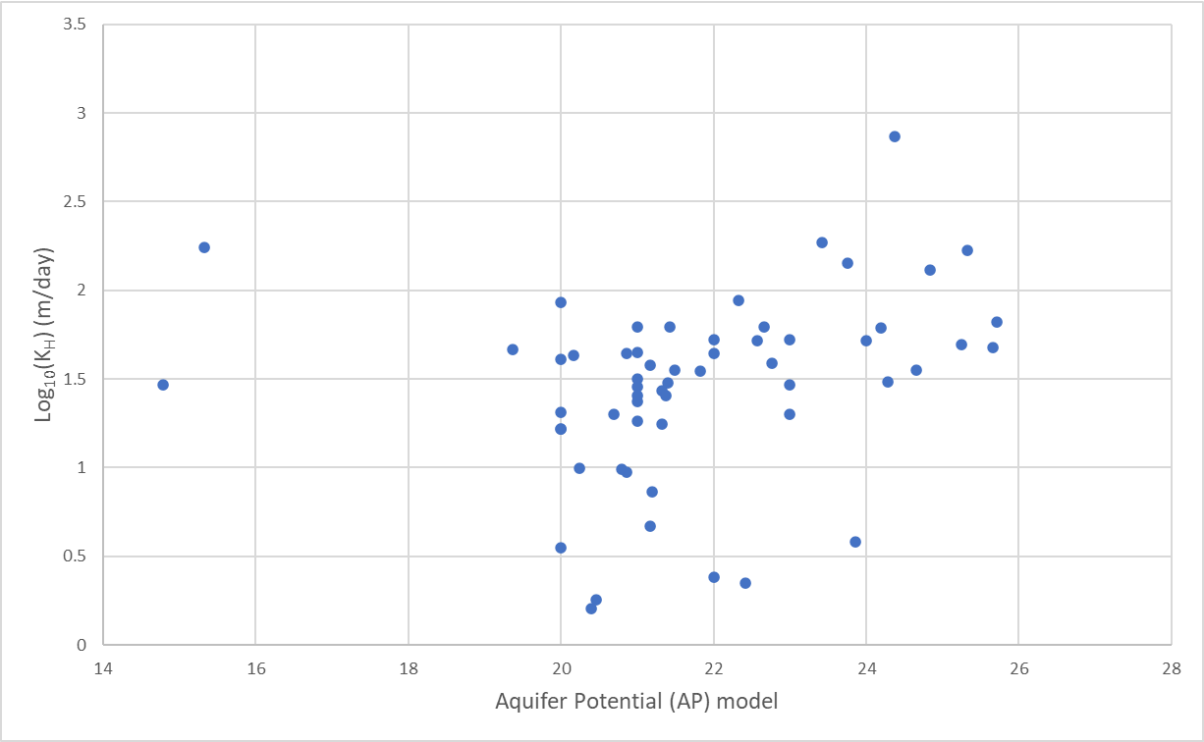

Figure 2.13 Horizontal hydraulic conductivity (K_H) versus Aquifer Potential (AP) model. Blue points are the estimates of K_H made from pumping test data (Section 2.1.7.1).

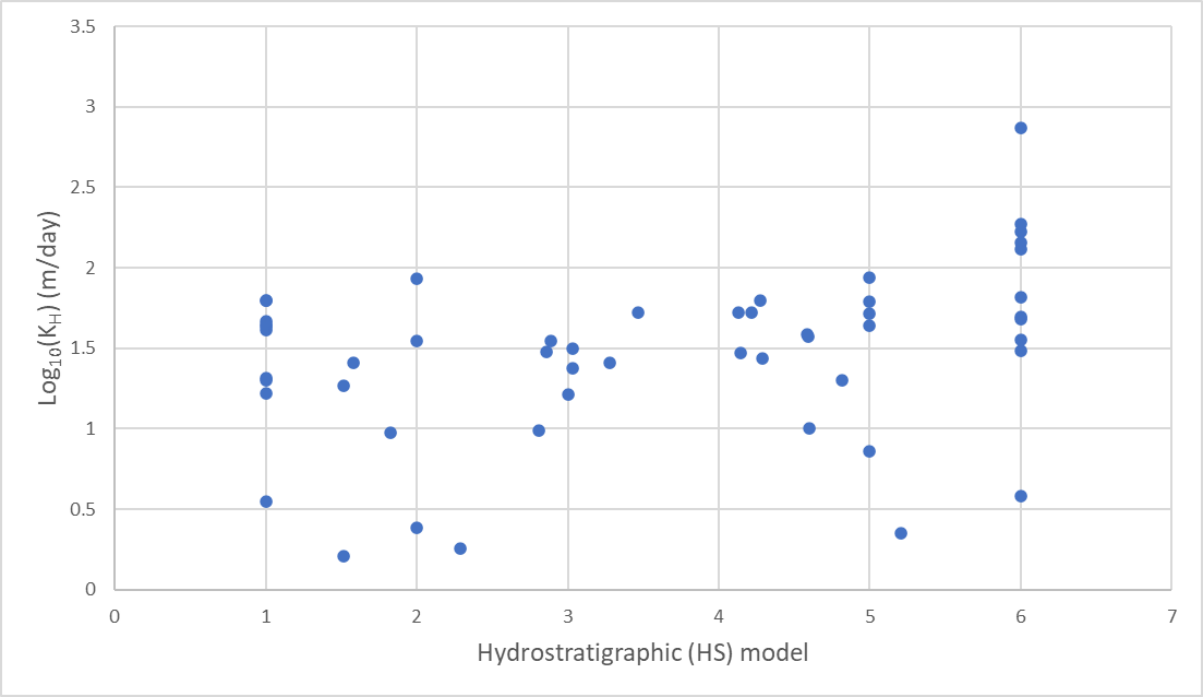

Figure 2.14 Horizontal hydraulic conductivity (K_H) versus Hydrostratigraphic (HS) model. Blue points are the estimates of K_H made from pumping test data (Section 2.1.7.1).

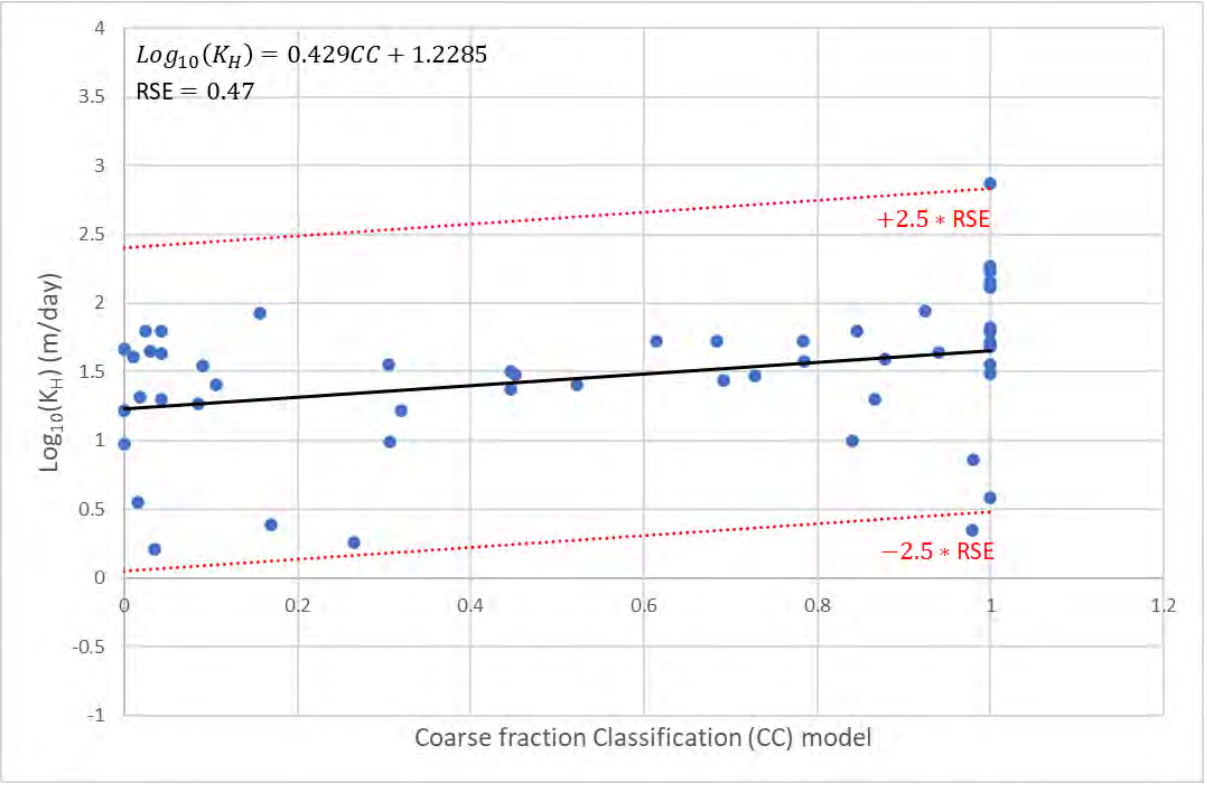

Figure 2.15 Horizontal hydraulic conductivity (K_H) versus Coarse fraction Classification (CC) model linear regression equation, as well as +/-2.5*RSE. RSE is an estimate of the variance of the error term for the equation fit to data, and 95% of values are expected to be found within 2*RSE. Blue points are the estimates of K_H made from pumping test data (Section 2.1.7.1).

2.1.7.3 Implementation

For the assessment in the Heretaunga Plains area as part of 3DAMP (Rawlinson 2023), the Heretaunga Plains groundwater flow model (Heretaunga GW model) was utilised for some iterative testing of K_H models. As 3DAMP is not working directly with a numerical groundwater model in the Ruataniwha Plains area, here, the method developed through iterative testing and expert knowledge for the Heretaunga Plains was utilised (Rawlinson 2023). This method utilised two synthetic data points to develop a linear relationship between K_H and the CC model, to overcome the limitation of low K_H values not being adequately represented due to the bias of the pumping test data towards high values (see Section 2.1.7.1).

This is achievable for the CC model as it is directly related to a physical property, however, it is not possible to do the same for the res model. As such, a high value was set at CC = 1 of K_H = 1,000 m/day (maximum K estimate from pumping test data in Ruataniwha was 950 m/day) and a low value at CC = 0.002 of K_H = 0.01 m/day. This low value is consistent with Rakowski and Knowling (2018), who found a lowest value in their calibrated Heretaunga groundwater flow model of K_H = 0.01 m/day, and also with literature values for silt (e.g. Section 2.1.7.1). Additionally,, for K_H values to be useful for numerical models, it is important to consider upscaling impacts (e.g. although literature values for clay are much lower, it is unlikely that a 100 x 100 m grid cell will be fully composed of such low K_H material). A linear trend was fitted to these points (Figure 2.16):

$$Log_{10}(K_H) = 5.01 * CC - 2.01 \quad \text{Equation 2.6}$$

Although four orders of magnitude uncertainty is required to fit all pumping test data with this equation (Figure 2.16), the validity of this relationship was further checked by comparing the K_H estimates from slug tests collected at 3DAMP_Well1 and 3DAMP_Well3 against coarse fraction estimates from either hand samples or lab-based grain-size analyses (Figure 2.17). The good correspondence between Equation 2.4 and these data (which aimed to sample the full range of permeability encountered in the wells) further supports the strong bias in the pumping test data towards high values and validity of the synthetic relationship developed (Figure 2.17).

Testing using the Heretaunga GW model with K_H values derived from a CC relationship highlighted that K_H values in the high range were still coming out too high as the CC model has less discrimination within the high value range (CC>0.9) than the res model (Rawlinson 2023). To overcome this limitation, a combined approach was used, taking the minimum value calculated from either the linear regression equation found with the resistivity model (Equation 2.6) or the synthetic relationship developed for the CC model (Equation 2.6). Where only one model exists, only that model was utilised to calculate K_H. Testing of these K_H values in the Heretaunga GW model and against expert knowledge provided suitable results (Rawlinson 2023, Hemmings 2023, Moore 2023). Here, this same combined approach was undertaken for the Ruataniwha Plains to calculate K_H. Previous numerical groundwater modelling in the Ruataniwha Plains found zones of calibrated K_H values between 0.7–60 m/day (Baalousha et al. 2010), which is consistent with the magnitude of K_H values calculated using this approach (see Section 3.0).

The relationships utilised assume that electromagnetic conduction in the area is primarily controlled by the amount of clay material present and so follow the same limitations as the hydrostratigraphic modelling – that this assumption is not valid in basement (consolidated) rock. Therefore, these areas are required to be dealt with in a different manner (see below for further details). Here, two different models were developed with different K_H values implemented for basement: *KH_initial* and *KH_initial_basehigh.*

To deal with the locations where there is data from only one model, a Boolean operator model (*KH_unc*) was developed: 0 corresponds to model cells with both CC and resistivity model data, and 1 corresponds to model cells with one or none of CC or resistivity model data. This model can be used to reflect the increase in uncertainty in these areas (*KH_unc* = 1).

As such, six models were developed, enabling further numerical GW model utilisation to be easily explored:

1. *K_res* $= 10^{0.8027 * \mathrm{Log}_{10}(\mathrm{res}) - 0.0322}$
2. *K_CC* $= 10^{5.01 * \mathrm{CC} - 2.01}$
3. *K_min* $= \min(\mathrm{K}_{\mathrm{res}}, \mathrm{K}_{\mathrm{CC}})$
4. *KH_initial* = KH_min (except where HU = 4, see below).
5. *KH_initial_basehigh* = KH_min (except where HU = 4, see below).
6. *KH_unc*: Boolean operator (0/1), where 1 identifies areas of higher uncertainty.

These calculations were made on the combined dataset, which now has columns *X, Y, Z, top_elev_HU, res, resvar, HU, CF, CF_STD, Cluster, Silhouette_Index, HS_unclipped, HS, facies*, *AP, aq, CC, K_res, K_CC, K_min, KH_initial, KH_initial_basehigh, KH_unc*.

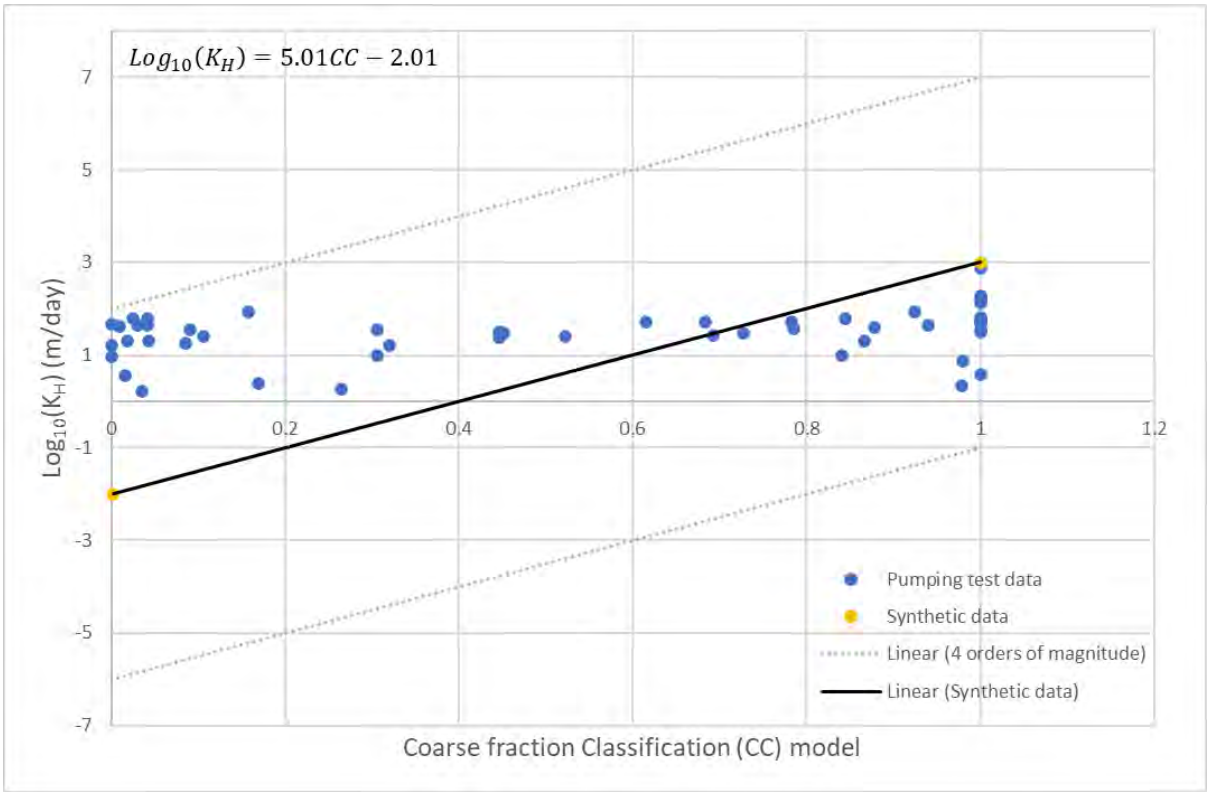

Figure 2.16 Horizontal hydraulic conductivity (K_H) versus CC model linear regression equation to synthetic data points developed from expert knowledge, as well as +/-4 orders of magnitude. Blue points are the estimates of K_H made from pumping test data (Section 2.1.7.1).

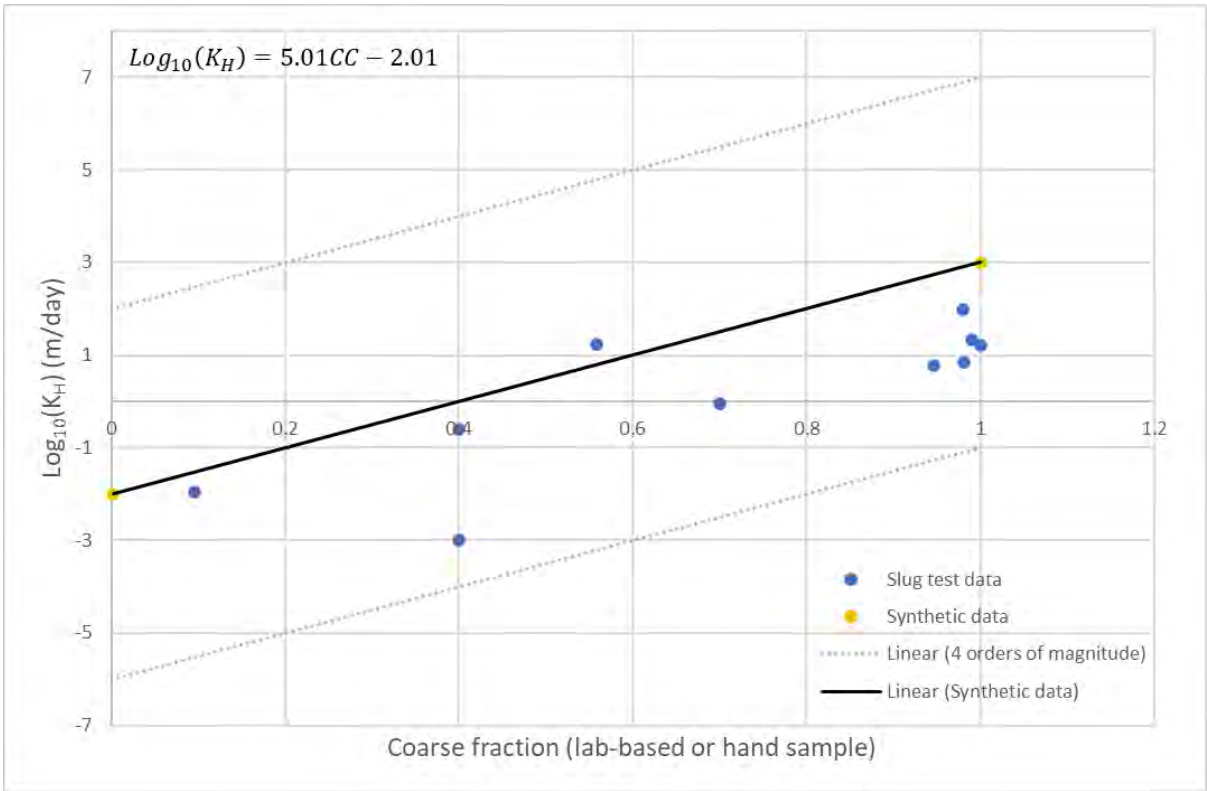

Figure 2.17 Horizontal hydraulic conductivity estimates (K_H) from slug tests at 3DAMP_Well1 and 3DAMP_Well3 versus coarse fraction estimates made from either hand samples or lab-based grain-size analyses (Lawrence et al. 2022a, 2022b) compared to the linear regression equation established between coarse fraction and K_H.

Consolidated K_H

As the relationships explored above are only relevant for the unconsolidated areas, for the consolidated material (HU4), literature values of K_H and information available from pumping tests in the areas were utilised (Section 2.1.7.1). Multiple models were developed to enable different use purposes.

Literature values (e.g. Freeze and Cherry 1979) were used to select a K_H value for consolidated material with low aquifer potential of 5 x 10^{-4} m/day. This could be suitable for a numerical groundwater model representing the basement as a no flow boundary, or for primarily assessing just K_H values relevant to unconsolidated sediments. As such, a *KH_initial* dataset was developed with all consolidated sediments mapped with $K_H = 5 \times 10^{-4}$ m/day.

To enable further explorations of potential connections with limestone and sandstone, a *KH_initial_basehigh* dataset was also developed with different values mapped for sandstone and limestone. Low aquifer potential was considered equivalent to mudstone/siltstone, medium aquifer potential equivalent to sandstone and high aquifer potential equivalent to limestone (Table 2.7). Where there was HU model information but no resistivity information, a low aquifer potential was assumed (Table 2.7).

Pumping test information in limestone provided K_H values between 1.6 and 134.3 m/day, with a mean of 42.5 m/day and median of 17.1 m/day. Pumping-test information in sandstone provided only one K_H value of 6.9 m/day. As these values are from pumping tests performed on water-bearing sandstone and limestone, they represent upper values for the sandstone and limestone material (e.g. medium to high aquifer potential).

Table 2.7 Horizontal hydraulic conductivity (K_H) mapping for consolidated sediments. HU = hydrogeological unit; CC = coarse-fraction classification; aq = simplified aquifer potential category.

HU	CC	aq	Assumption	*KH_initial* (m/day)	*KH_initial_basehigh* (m/day)
4	0.0001–0.0009	cl	Mudstone/siltstone	5 x 10^{-4}	5 x 10^{-4}
4	0.0010–0.0011	cm	Sandstone	5 x 10^{-4}	6.9
4	0.0012–0.0014	ch	Limestone	5 x 10^{-4}	17.1
4	N/A	N/A	Basement	5 x 10^{-4}	5 x 10^{-4}

2.1.8 Data Formats

The 3D model datasets were combined within a point *.csv* file, with x,y,z defining the centre of each grid cell. Attribute columns relate to each of the different 3D models. This format was developed for serving the data on an online webmap. The format provides quick access to all datasets for cross-section and virtual borehole visualisations, as all datasets reference the same x,y,z locations. Additionally, a selection of the 3D models was exported to individual *x,y,z,value .csv* files to enable 3D visualisation as individual block models within a Leapfrog viewer file.

A selection of the 3D models was also converted into multi-band raster files, enabling further accessibility, such as visualisation of elevation slices within GIS software and easy utilisation by numerical groundwater models. Each multi-band raster contains 500 bands in elevation order, where Band 1 = 651 mASL and Band 500 = -349 mASL, with each band consisting of a 2-m-thick vertical slice referenced to the cell centre (i.e. Band 1 = 650–648 mASL). This elevation information is included within the metadata of the files.

2.2 2D Maps

2.2.1 Aquifer Thickness

In this section, a simplifying assumption is made that an aquifer corresponds to >50% coarse material (CC >0.5) and an aquitard corresponds to ≤50% coarse material (CC ≤0.5), see Sections 2.1.3 and 2.1.6.

This is similar to Hansen et al. (2016), who used a definition of at least 50% clay to define aquitard material. Hydrogeological interpretations of SkyTEM data were previously used by Hansen et al. (2016) to find a correlation between aquifer vulnerability to surface nitrate contamination in Denmark and the thickness of material with more than 50% clay in the upper 30 m (interpreted from the SkyTEM data and compared to measured nitrate values).

Total Aquifer Thickness Maps

All model cells with CC >0.5 were selected and the vertical thickness summed for each horizontal cell. This information was converted to a raster file to provide a total aquifer thickness map (Figure 3.4). This process ignores any complexity of multi-layered aquifers that may be separated by aquitards and highlights only the total thickness of aquifer material.

The total aquifer thickness raster file was converted to polygons of aquifer thickness and aquifer extents. To simplify the aquifer extent polygon, any polygon parts smaller than 1 km were eliminated (Figure 3.4).

The total aquifer thickness was divided by the full thickness of unconsolidated sediments for each horizontal cell and multiplied by 100. This information was converted to a raster file to provide a map of the percentage of unconsolidated sediments classified as an aquifer (Figure 3.4).

Surficial and Deep Aquifer Thickness Maps

Horizontal cells that had CC >0.5 at the land surface were selected and the vertical thickness directly beneath of CC >0.5 summed for each of these horizontal cells. If any two consecutive cells (total of 4 m thickness) with CC ≤0.5 were encountered, then the thickness summation ceased. This information was converted to a raster file to provide a surficial aquifer thickness map (Figure 3.4).

The difference between the total aquifer thickness and the surficial aquifer thickness was calculated. This information was converted to a raster file to provide a deep aquifer thickness map (Figure 3.4).

2.2.2 Aquitard Thickness

CC ≤0.5 was used to assess the thickness of aquitard material in the unconsolidated sediments in the upper 100 m (Figure 3.6). To remove the potential of including basement material (particularly relevant in shallow river valleys where the unconsolidated thickness is relatively shallow and there is a higher uncertainty on the basement clipping surface that was used), cumulative thickness was only calculated if there was at least one cell greater than the CC threshold encountered beneath the aquitard units (i.e. an aquitard was only defined where there is an underlying aquifer).

2.2.3 Near-Surface Properties

Near-surface property estimates are important for a number of purposes, including improving understanding of groundwater–surface water interaction and guiding riverbed conductance values for numerical groundwater modelling.

Both the harmonic mean and geometric mean were calculated for the upper 5 m, 10 m, 15 m, 20 m, 30 m and 50 m for the *res, resvar, CC, KH_initial* and *KH_initial_basehigh* models. Each dataset was converted to a raster file to provide indicator maps of near-surface properties (Figure 3.5).

2.2.4 Horizontal Hydraulic Conductivity Maps

To provide an estimate of horizontal hydraulic conductivity through the full thickness of the model area, the KH models from Section 2.1.7 were used to calculate both the geometric mean and harmonic mean of horizontal hydraulic conductivity through the vertical column of unconsolidated sediments (HU2) and through basement (HU4) where this was present at the surface. This information was converted to raster files (Figure 3.7). The geometric mean is useful to understand average horizontal flow properties, while the harmonic mean highlights the influence of lower permeable material and is related to vertical flow properties.

For comparison with other studies, the geometric mean and harmonic mean *KH_initial* for the upper 40 m, 75 m and 100 m were also calculated.

3.0 RESULTS AND DISCUSSION

3.1 3D-Gridded Model Development

Three-dimensional model datasets were combined within a *.csv* file, with x,y,z defining the centre of each grid cell, and including the following parameters: *X, Y, Z, top_elev_HU, res, resvar, HU, CF, CF_STD, Cluster, Silhouette_Index, HS_unclipped, HS, facies*, *AP, aq, CC, K_res, K_CC, K_min, KH_initial, KH_initial_basehigh, KH_unc* (Table 3.1; Figures 3.1–3.4). A selection of these models was converted to multi-band raster format, enabling further accessibility, such as visualisation of elevation slices within GIS software and easy utilisation by numerical groundwater modelling.

The 3D models utilise 100 x 100 m grid cells horizontally and 2-m-thick grid cells vertically. Grid cells are defined in elevation (relative to mean sea level) rather than in depth (relative to the ground surface), so exact clipping at the surface varies based on the grid location versus the DEM location. A 25 m resolution DEM was used for surface clipping (Sahoo et al. 2023).

A summary of the developed models is provided below:

- An interpolated resistivity (res) model, which interpolated the SkyTEM-derived smooth resistivity model and available resistivity models from ground-based surveys to the regular grid. Model gaps remain at distances greater than 500 m from any resistivity data and below the calculated standard depth of investigation.
- A major Hydrogeological Unit (HU) model, which utilised the previously developed manually delineated major hydrogeological unit surface to split the 3D grid into two units. The surfaces were developed using interpolation, which fills any gaps in the resistivity data.
- A Hydrostratigraphic (HS) model, which utilised the previously developed six-cluster model, and utilised the basement HU to restrict the model to only the unconsolidated sediments (where the hydrostratigraphic modelling assumptions are valid). The hydrostratigraphic modelling enabled a variable relationship between resistivity and permeability across the study area, using clay fraction (CF) as an indication of permeability. It also used the sharp resistivity model.
- A resistivity facies (facies) model, which separated the res model into 14 $\log_{10}$-based uniform intervals, to group materials that are expected to have similar hydrologic and geologic properties based on their resistivity (to assist with easier discrimination of significant variability and similarity). Model gaps are the same as in the res model.
- An Aquifer Potential (AP) model, which has 28 classes and utilised the HU and facies models to separate the model into likely consolidated sediments (basement; 14 classes) and likely unconsolidated sediments (14 classes), whilst providing an indicator of the likelihood of each model cell to host aquifer-bearing material (after assessments against other datasets such as lithological logs). This model utilised the same relationships between resistivity and permeability across the entire study area. Model gaps are the same as in the res model.
- A Coarse fraction Classification model (CC), which utilises the CF model for the unconsolidated sediments and the AP model for the consolidated sediments, providing a 0–1 model of estimated coarse fraction. It was primarily developed to support hydraulic conductivity estimates for numerical modelling. The coarse fraction estimates from the CC model performed well in defining aquifer and aquitard material, compared with lab-based coarse fraction measurements from seven bores that had this data available.

- Horizontal Hydraulic Conductivity models (KH), calculated for the unconsolidated sediments using an empirical relationship between horizontal hydraulic conductivity estimates from pumping tests and the res model, and an expert-knowledge-guided relationship with the CC model (following an approach developed using numerical groundwater flow model testing in the Heretaunga Plains [Rawlinson 2023]). Previous numerical groundwater modelling in the Ruataniwha Plains found zones of calibrated K_H values between 0.7–60 m/day (Baalousha et al. 2010), which is consistent with the magnitude of K_H values calculated using this approach. Literature values, expert knowledge and local pumping test information were used to assign discrete values for the consolidated sediments, with two different associated models developed.

The models developed are limited by the supporting datasets available, such as lithological logs, grain-size estimates and hydraulic conductivity estimates from pumping test data. Uncertainty increases with increased distance from such supporting datasets. There are limited supporting datasets deeper than 40 m depth (e.g. Tschritter et al. 2022; Kellett et al. 2023), and, as such, uncertainty increases with depth.

Note that, due to the uniform 3D gridding approach taken, resolution is lost along flight lines where the original SkyTEM-derived resistivity models have finer resolution. See Figure 2.2 for a zoomed-in example showing the difference in resolution between the original and gridded datasets. However, given the primary applications of groundwater modelling and online visualisation of the entire datasets, the approach taken is considered appropriate for these applications. The same methodology could be used to create finer-resolution small subsets of the data; otherwise, different gridding approaches could be tested, such as non-uniform gridding within different software or scripting.

The HU model utilised a manually delineated surface, described within Sahoo et al. (2023). The use of this manual surface results in some resolution limitations of the HU model in contrast to the HS model. However, the HS model is not able to distinguish between the high resistivity from limestone rather than from unconsolidated gravel, for instance; hence clipping by the manual surface is required when working with the entire aquifer dataset. Subsequent studies in small, localised areas may wish to utilise the unclipped HS model to assess basement resolution, which is why both the *HS_unclipped* and *HS* column are provided. It is important to be aware that, although the *HS_unclipped* model seems to map basement well, where basement corresponds to low resistivity material, such as mudstone and siltstone, where basement is high resistivity, such as limestone, it is misleading and should not be used.

The CC and res models were selected to derive the horizontal hydraulic conductivity datasets. The CC model relates to a single physical property and so enables an expert-informed relationship to be developed, while the resistivity model retains the finest resolution, both spatially and numerically. Although there was a generally linear trend in the relationships found between the 3D models and horizontal hydraulic conductivity, there was a wide band of values around these and the value of the pumping test dataset for this assessment was limited due to its bias towards high values. Slug tests and grain size estimates from the 3DAMP drilling programme, which targeted the full range of permeability encountered, enabled a valuable unbiased assessment that supported the coarse fraction relationship to hydraulic conductivity developed. Likely the best methodology to utilise these data in a numerical model will enable a variable trend throughout the model to allow for spatial variations – e.g. associated with changing depositional environments.

As the best model domain and methodologies of averaging (upscaling) properties of K_H within numerical groundwater models depend on the questions being asked of the model (type of scenario), it is expected that the selection of the inclusion method of these datasets within numerical groundwater modelling may depend on the question being explored. For example, two different K_H models were developed to support different basement constructions within numerical models.

Table 3.1 Summary of 3D model names and descriptions.

Attribute	Description	Type	Comments
X	Easting in NZTM of the centre of the model cell.	Numerical	100 m horizontal cell resolution
Y	Northing in NZTM of the centre of the model cell.	Numerical	100 m horizontal cell resolution
Z	Elevation (m ASL) in NZVD2016 of the centre of the model cell.	Numerical	2 m vertical cell resolution
top_elev_HU	Elevation (m ASL) in NZVD2016 of the centre of the highest Z cell at this X,Y location that has HU data.	Numerical	See Section 2.1.2
res	Resistivity (ohm.m).	Numerical	See Section 2.1.1
resvar	Kriging variance of the resistivity model.	Numerical	See Section 2.1.1
HU	Major hydrogeological units.	Categorical: 2,4	See Section 2.1.2
CF	Clay Fraction.	Numerical: 0–1	See Section 2.1.3
CF_STD	Clay Fraction Standard Deviation.	Numerical	See Section 2.1.3
Cluster	Hydrostratigraphic model – not clipped by basement – interpolated with 200 m radius.	Categorical: 1–6	See Section 2.1.3
Silhouette_Index	Silhouette index for *Cluster*.	Numerical	See Section 2.1.3
HS_unclipped	Hydrostratigraphic model – not clipped by basement.	Categorical: 1–6	See Section 2.1.3
HS	Hydrostratigraphic model – clipped by basement.	Categorical: 1–6	See Section 2.1.3
facies	Resistivity facies model.	Categorical: 1–14	See Section 2.1.4
AP	Aquifer potential model.	Categorical: 1–28	See Section 2.1.5
aq	Simplified aquifer potential model.	Categorical: cl, cm, ch, ul, um, uh	See Section 2.1.5
CC	Coarse-fraction Classification model.	Numerical: >0.002–1 Categorical: 0.0001–0.0014	See Section 2.1.6
K_CC	Horizontal hydraulic conductivity (m/day) estimate from the CC model	Numerical	See Section 2.1.7
K_res	Horizontal hydraulic conductivity (m/day) estimate from the res model	Numerical	See Section 2.1.7

Attribute	Description	Type	Comments
K_min	Horizontal hydraulic conductivity (m/day) estimate, min(*K_CC*, *K_res*); where facies ≤4, *KH_min* = *K_CC*.	Numerical	See Section 2.1.7
KH_initial	Horizontal hydraulic conductivity (m/day) estimate of initial value (*K_min* and 5×10^{-4} assigned to all consolidated sediments).	Numerical	See Section 2.1.7
KH_initial_basehigh	Horizontal hydraulic conductivity (m/day) (*K_min* and higher values assigned to likely sandstone and limestone).	Numerical	See Section 2.1.7
KH_unc	Estimate of areas of higher uncertainty (*KH_unc* = 1) for horizontal hydraulic conductivity estimates.	Categorical: 0,1	See Section 2.1.7

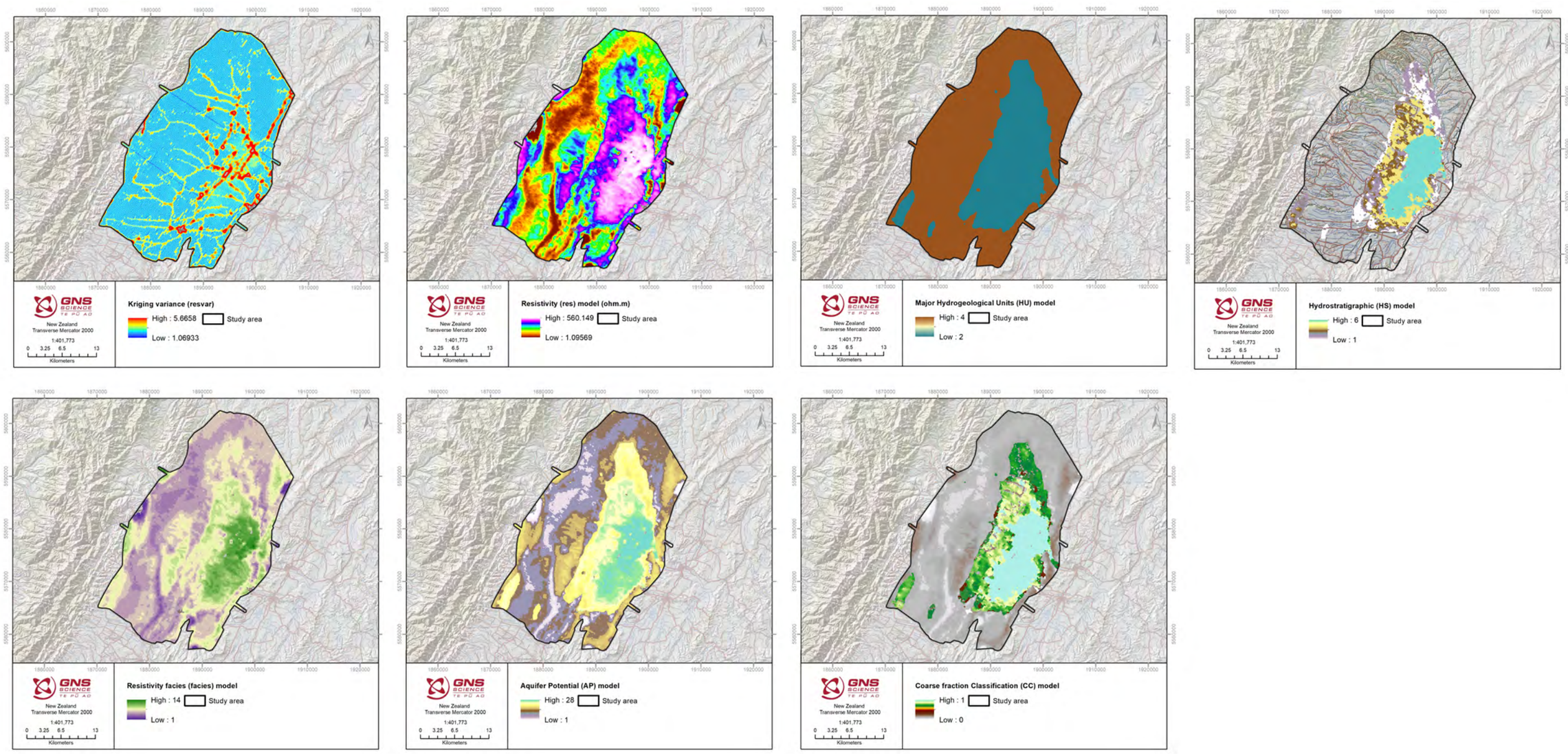

Figure 3.1 Three-dimensional models, map view at 141 mASL. See Sections 2.1.1–2.1.6 for model details.

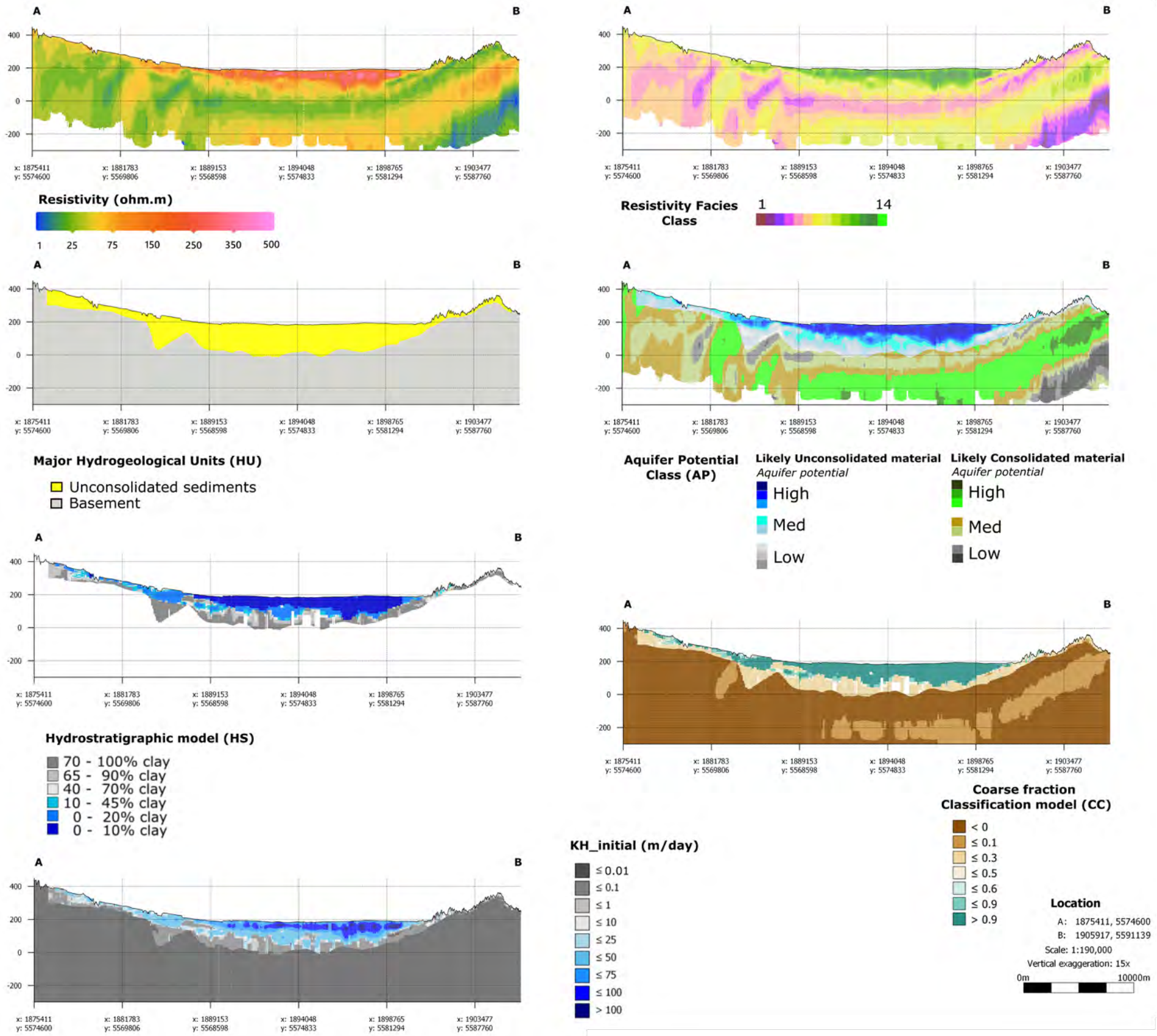

Figure 3.2 Three-dimensional models shown across profile A–B. Cross-section location is shown in Figure 2.1. See Sections 2.1.1–2.1.7 for model details.

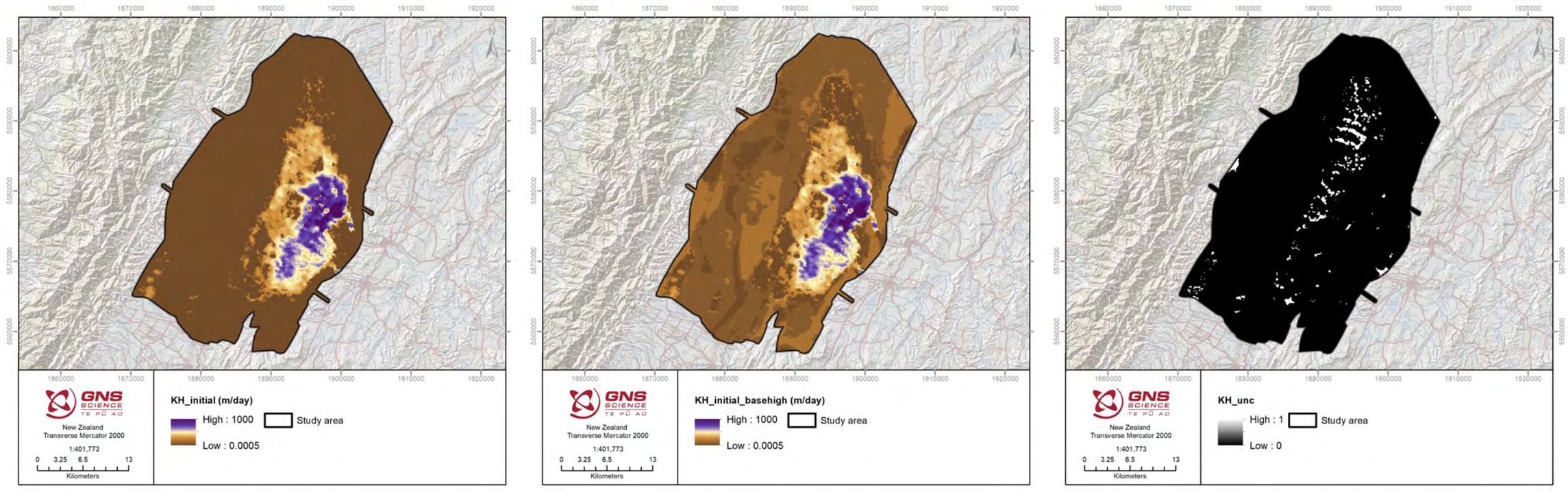

Figure 3.3 Three-dimensional models of horizontal hydraulic conductivity, map view at 141 mASL. See Section 2.1.7 for model details.

This page left intentionally blank.

3.2 2D Maps

Simplifications of the 3D models to 2D maps can assist with more readily investigating various aspects of the Ruataniwha Plains aquifer system.

2D maps/models derived, primarily using the CC model, include:

- Aquifer thickness, separated into surficial, deep, total and total as a percentage of unconsolidated thickness (Figure 3.4). This process ignores any complexity of multi-layered aquifers that may be separated by aquitards and highlights only the total thickness of aquifer material.
- Near-surface properties (res, CC and K_H; Figure 3.5) for the upper 5 m, 10 m, 15 m, 20 m, 30 m and 50 m, using geometric and harmonic means.
- Aquitard thickness (Figure 3.6).

Geometric and harmonic means of horizontal hydraulic conductivity (K_H) through the full vertical column of unconsolidated sediments and full vertical column of consolidated sediments where these are present at the surface (Figure 3.7). The geometric mean is useful to understand average horizontal flow properties, while the harmonic mean highlights the influence of lower permeable material and is related to vertical flow properties.

This page left intentionally blank.

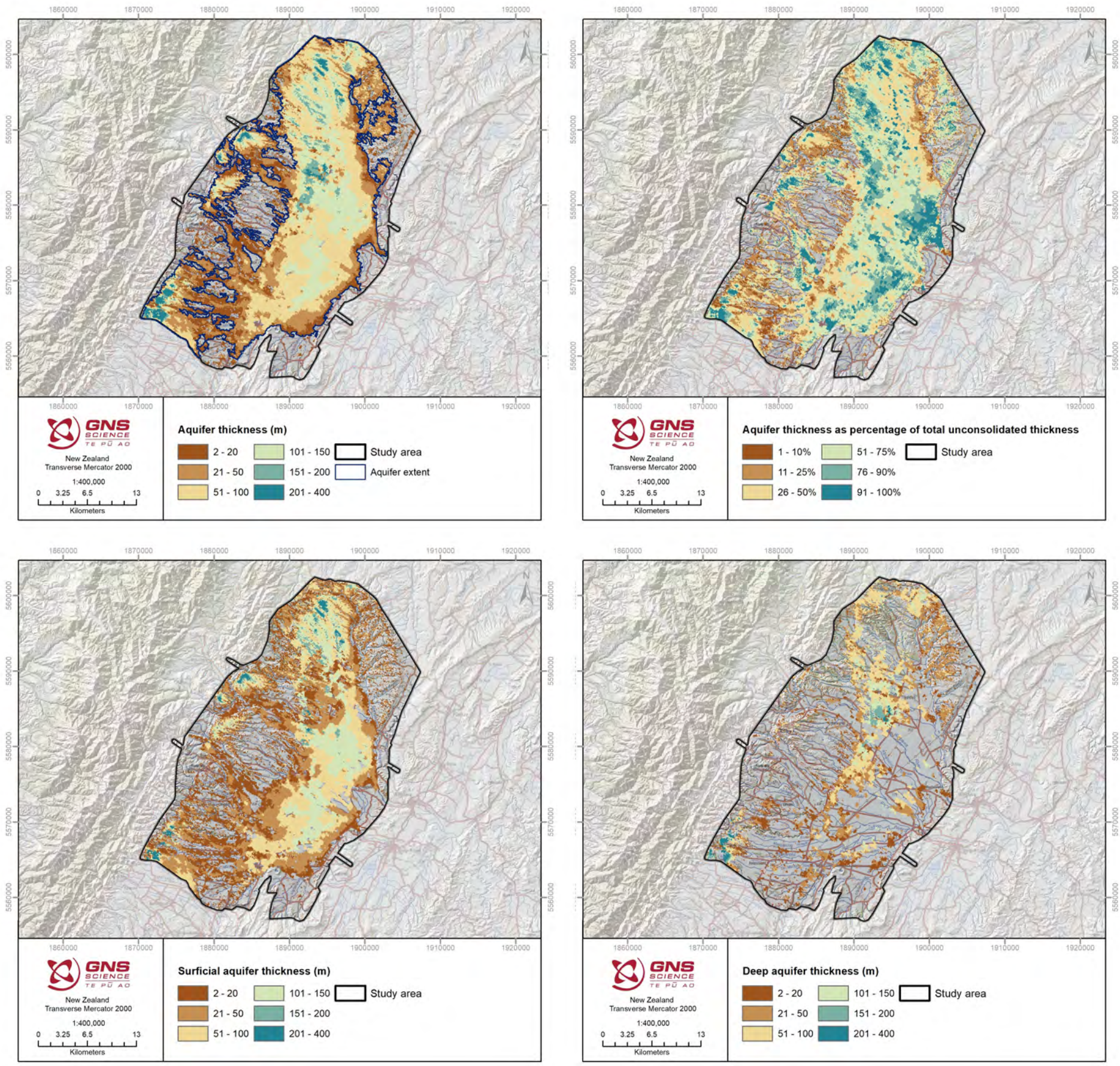

Figure 3.4 Aquifer thickness maps. (Top left) Aquifer thickness and aquifer extent polygon; (top right) aquifer thickness as a percentage of total unconsolidated thickness; (bottom left) surficial aquifer thickness; and (bottom right) deep aquifer thickness. All are calculated from model cells with CC >0.5. See Section 2.2.1 for further details.

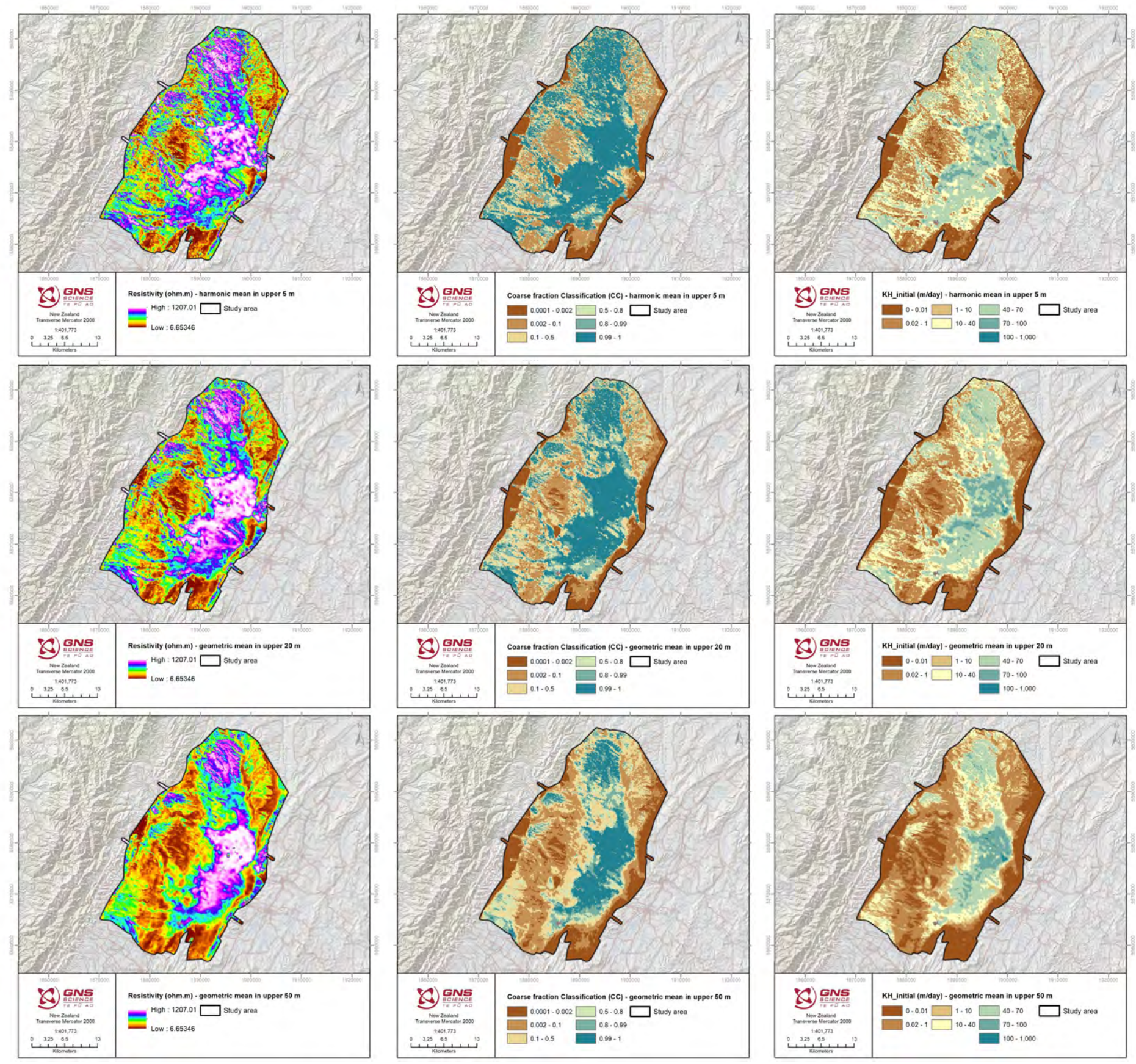

Figure 3.5 A selection of near-surface property estimates. Columns from left to right: (left column) resistivity (ohm.m); (middle column) coarse-fraction classification; (right column) initial horizontal hydraulic conductivity (*KH_initial* [m/day]). Rows from top to bottom: (top row) harmonic mean of upper 5 m; (middle row) geometric mean of upper 20 m; (bottom row) geometric mean of upper 50 m.

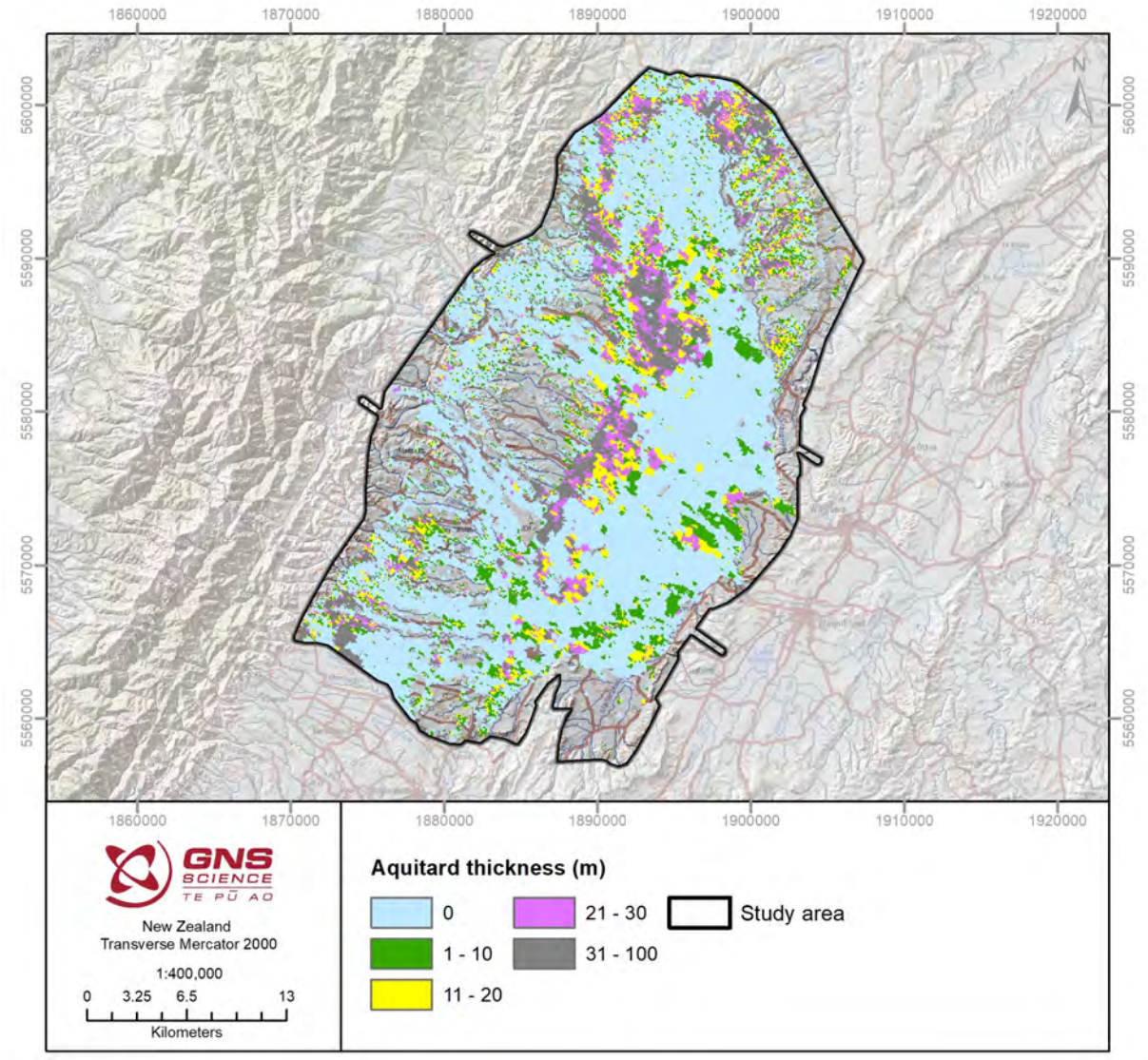

Figure 3.6 Aquitard thickness in the upper 100 m. See Section 2.2.2.

This page left intentionally blank.

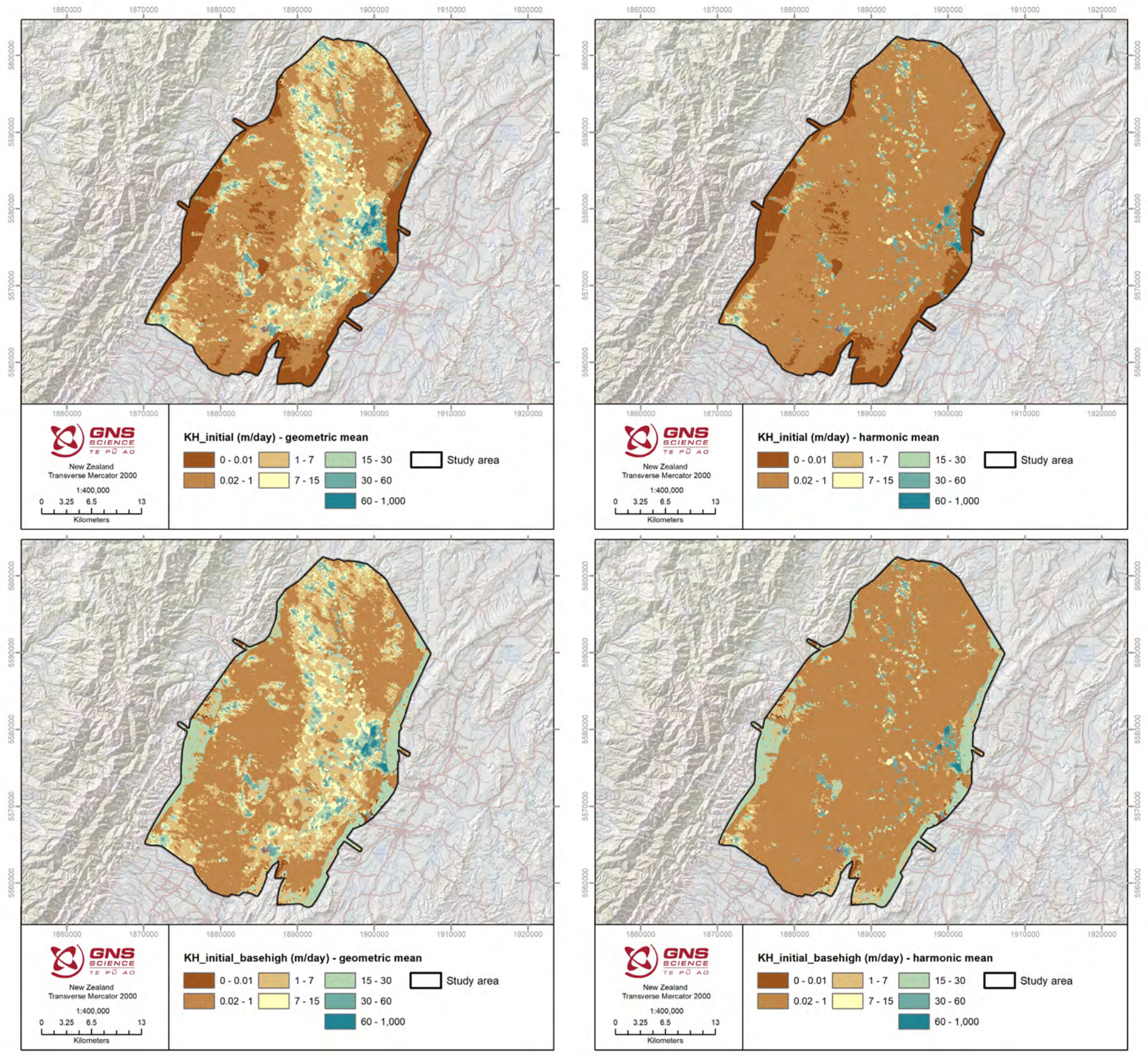

Figure 3.7 Geometric and harmonic mean of *KH_initial* and *KH_initial_basehigh*, calculated through each vertical 3D model column corresponding to unconsolidated sediments, and to consolidated sediments where these are at the surface.

This page left intentionally blank.

3.3 Comparison to Previous Investigations

The models and maps developed can assist with further hydrogeological understanding of the Ruataniwha Plains aquifer system. Here, a few comparisons are made to previous studies.

PDP (2018) aimed to provide aquifer property data, in particular hydraulic conductivity and storage, for the development of a new groundwater flow model for the Ruataniwha Basin. As part of that work, PDP (2018) reviewed existing pumping test data in the Ruataniwha Basin, reanalysed tests to derive additional information, and provided graphs and maps detailing the distribution of observed hydraulic properties in the Basin. For the review and reanalysis, PDP (2018) split the bores into three categories using the top of the screen where it was available, or the bore depth. The resulting 'depth' categories were: 5–40 m, 40–75 m, and >75 m. Zone polygons for a lower transmissivity zone (250–1000 m^2/day) and a higher transmissivity zone (>1000 m^2/day) were delineated manually based mainly on the distributions of medium-high confidence parameters. These polygons are displayed in Figure 3.8 along with the geometric mean of the *KH_initial* model for the upper 40 m, 75 m and 100 m. The two datasets show very good agreement, with the *KH_initial* model providing additional refinement to boundaries of the zones with higher permeable material. This is particularly true for the >1000 m^2/day polygon, where the *KH_initial* model shows an extension of higher permeability material to the north-east, and movement of this zone to the north-east with depth.

Figure 3.8 also highlights the location of previously noted paleochannels through the area. The upper 40 m map identifies paleochannels in the south, near Takapau, previously identified by Francis (2001). The upper 100 m map highlights deeper paleochannels north of Ongaonga, previously noted by Francis (2001) and PDP (2018), however, Figure 3.8 highlights the previously unknown full extent of these channels, which may assist with targeting drilling for new water sources through this area.

A shallow aquitard comprising dominantly clay-bound gravel, the "Shallow Tukipo Aquitard/Aquiclude", was identified by PDP (1999) up to a depth of 80 m within Recent Terrace Aquifer Group deposits between the Tukituki and Makaretu rivers. Brown (2002) concluded that this 'aquitard' probably consists of "poorly sorted last glaciation and older late Quaternary gravel deposits and is not a valid unit to be retained for aquifer grouping". However, through subsequent conceptualisations, the deposits have still been assumed to act as an aquitard in this area (e.g. previous conceptualisations as summarised by Harper 2018). The aquitard thickness calculated (Figure 3.6; Figure 3.9) was compared with locations where the Tukipo Aquitard/Aquiclude was identified in boreholes by PDP (1999). Although there is some correlation between these, no large-scale continuous aquitard has been identified in the models in this report (e.g. Figure 3.6; Figure 3.9). Additionally, through detailed assessments (i.e. keyword searches and manual checks of lithology descriptions in bores identified by PDP [1999] and cross-checked against report descriptions and interpretations referencing these) of lithological descriptions as part of 3DAMP (Herpe and Rawlinson 2023), relevant descriptions such as "claybound" or "cemented" could not be found in all wells previously identified as containing an aquitard, and gravel layers that were found to have descriptors of "claybound" or "cemented" were left as "unknown" rather than being defined as an "aquitard" during the clay fraction modelling (Herpe and Rawlinson 2023). It is possible that information has been lost in the digital lithological log database compared with the original driller's well logs. However, high-resistivity values were found in these areas, indicating an insufficient volume of clay material to reduce the resistivity. This could possibly occur due to the binding material consisting of pumice-derived fine material (silica-rich), primarily in the reworked old terraces, being the "cemented" gravels of the aquitard. The models in this report support the

Brown (2002) conclusion that the Tukipo Aquitard/Aquiclude is unlikely to be a valid unit for aquifer grouping, and the extent and significance of this unit may currently be over-stated; however, further investigations may be needed to confirm the resistivity, mineralogical and hydrogeological character of any fine cementing material in the area.

The aquitard thickness calculated (Figure 3.6) was also compared to locations of boreholes that had ever recorded artesian pressures (Figure 3.9; Harper 2024). Artesian pressures in Ruataniwha Plains are strongly linked to temporal conditions, for example, in the Jan/Feb 2020 water level survey, only bore 16490 recorded artesian pressures (Tschritter et al. 2022). In Figure 3.9, an aquitard is identified overlying, or immediately adjacent to, all the northernmost bores, as well as bore 2043 (eight bores total). Bores 15015, 16490, 1869, 3452 and 16486 do not have an immediately obvious connection to the identified aquitard units. Although bore 15015 has no screen, depth or lithology information, the other four bores are all screened deeper than 70 m. It's possible that at these depths, artesian pressures are not caused by local conditions, but are influenced by the topographic highs and aquitard layers identified to the northwest of the bores. An example of this is shown in Figure 3.9 (cross-section through bore 16490 and *KH_initial* model). However, bore 16490 also specifically describes clay derived from limestone and pumice. As above, further investigations may be needed to confirm the resistivity, mineralogical and hydrogeological character of any fine cementing material in the area to assess if resistivity contrasts are expected between the aquifer and aquitard material in the area.

A Concurrent Gauging Programme was undertaken in 2008/2009 (Johnson 2011) and Figure 3.10 shows the derived surface water flow patterns compared to the upper 5 m of the K_H models. Conservative (no gain or loss) patterns can be seen where the *KH_initial* model shows low permeability. Losing reaches are seen where the *KH_initial* model shows high permeability. There is a less clear pattern for gaining reaches, although they seem to occur in areas with *KH_initial* properties varying along the reach between low, medium and high values. Comparison to the *KH_initial_basehigh* model suggests gaining reaches in the southeast may be associated with flux from limestone. Morgenstern et al. (2012) found clear river recharge signatures in isotope and gas measurements only near the lower reaches of the Waipawa and Tukituki rivers, which is consistent with the higher permeability material shown in the *KH_initial* model at these locations in Figure 3.10.

The previous hydraulic conductivity to resistivity relationship developed in the Ruataniwha Plains by Meilhac et al. (2009) was estimated on a fairly limited number of data points and resistivity range using slug tests and nanoTEM data (see Section 2.1.7). For the resistivity range investigated (~200–700 ohm.m), the Meilhac et al. (2009) relationship provides hydraulic conductivity values with the same order of magnitude to the relationship developed in this report (Table 3.2). However, for values below the resistivity range investigated, the Meilhac et al. (2009) relationship estimates negative values (Table 3.2). This further highlights the importance of developing such relationships utilising a wide range of resistivity values and hydraulic conductivity estimates from pumping tests, and to be aware of any data range limitations.

Overall, the maps and models developed provide useful information to improve understanding of the hydrogeological system in the Ruataniwha Plains, support a greater understanding of other datasets (e.g. pumping test and stream flow gauging data) and could be used to guide additional data collection with greater precision.

Table 3.2 Comparison of horizontal hydraulic conductivity (K_H) values for a selection of resistivity values, estimated from the relationship developed by Meilhac et al. (2009) and the relationship developed in this report (Equation 2.4).

Resistivity (ohm.m)	K_H (m/day) (Meilhac et al. 2009)	K_H (m/day) (Equation 2.4)
50	-112	22
100	-60	37
200	44	65
700	562	179

This page left intentionally blank.

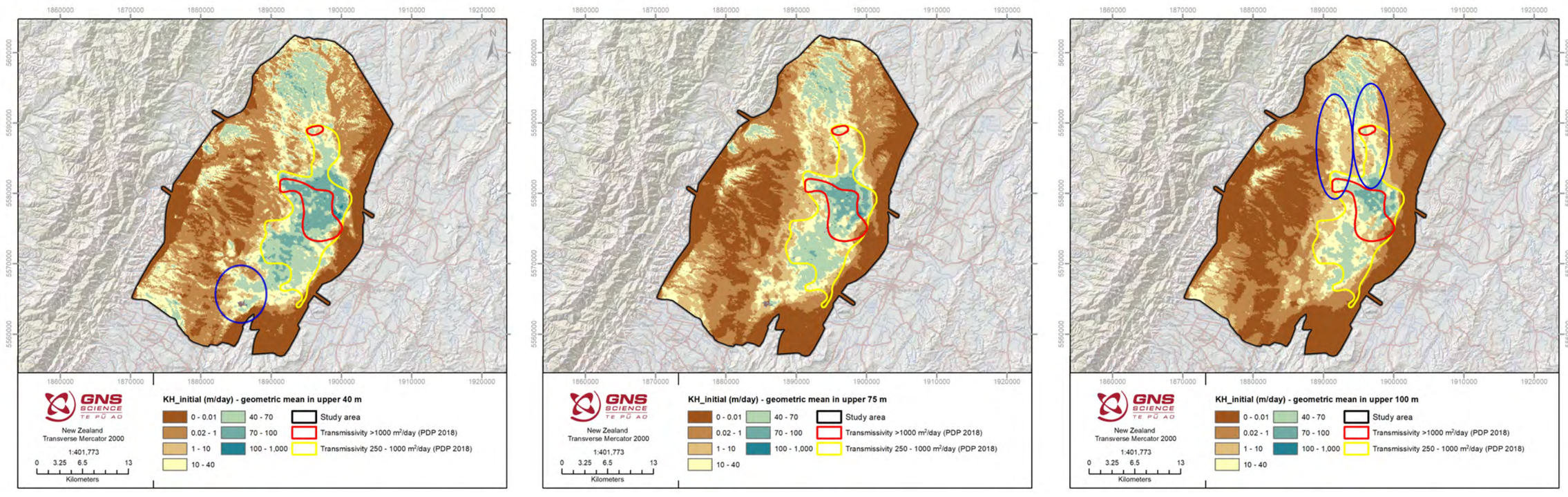

Figure 3.8 Estimated horizontal hydraulic conductivity (*KH_initial*). (From left to right) in the upper 40 m, 75 m and 100 m, compared with zones of high transmissivity developed by PDP (2018) through assessments of pumping test data. Blue ellipses identify areas discussed in the text.

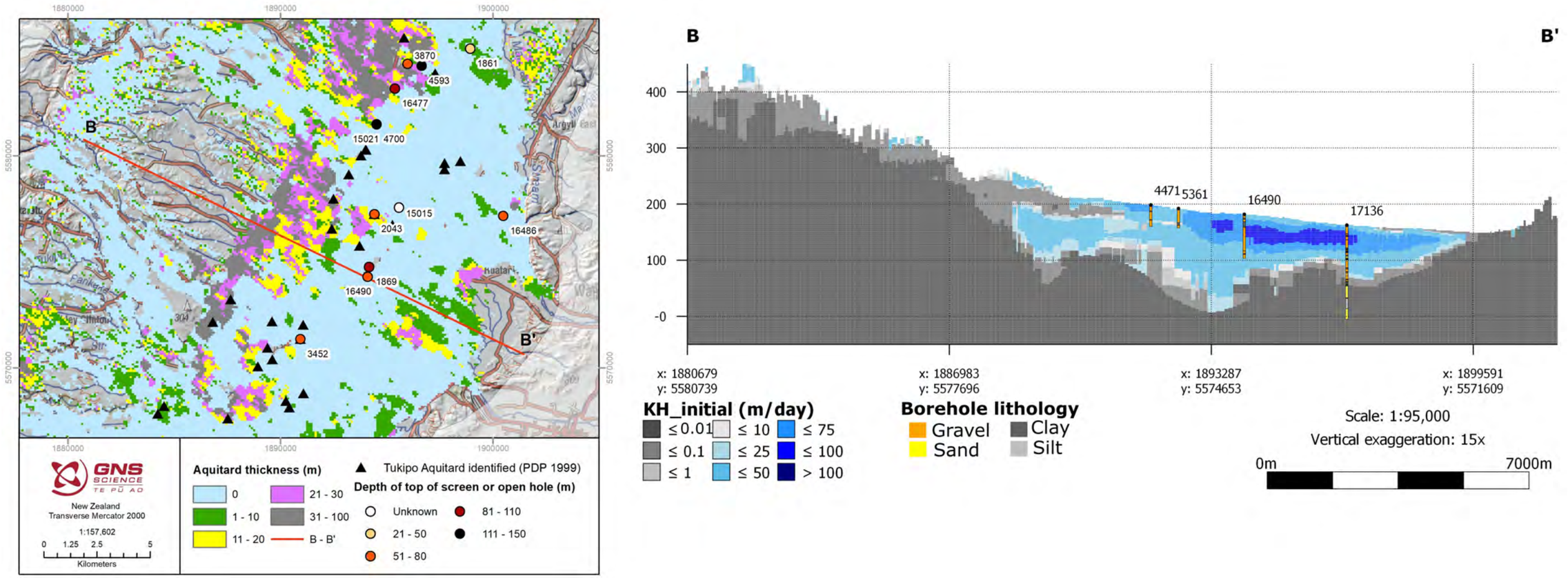

Figure 3.9 Comparison of artesian bores to aquitard thickness and hydraulic conductivity. (Left) Zoom-in showing comparison of aquitard thickness in the upper 100 m to bores that have had a water level recorded above land surface at least once (Harper 2024) and where the Tukipo Aquitard was previously identified (PDP 1999). (Right) Cross-section B-B' showing hydraulic conductivity (*KH_initial*) and a selection of boreholes. Borehole 16490 (screened near the base of the bore) was identified as having artesian pressures during the Jan/Feb 2020 water level survey that was undertaken coincident with the SkyTEM data collection (Tschritter et al. 2022).

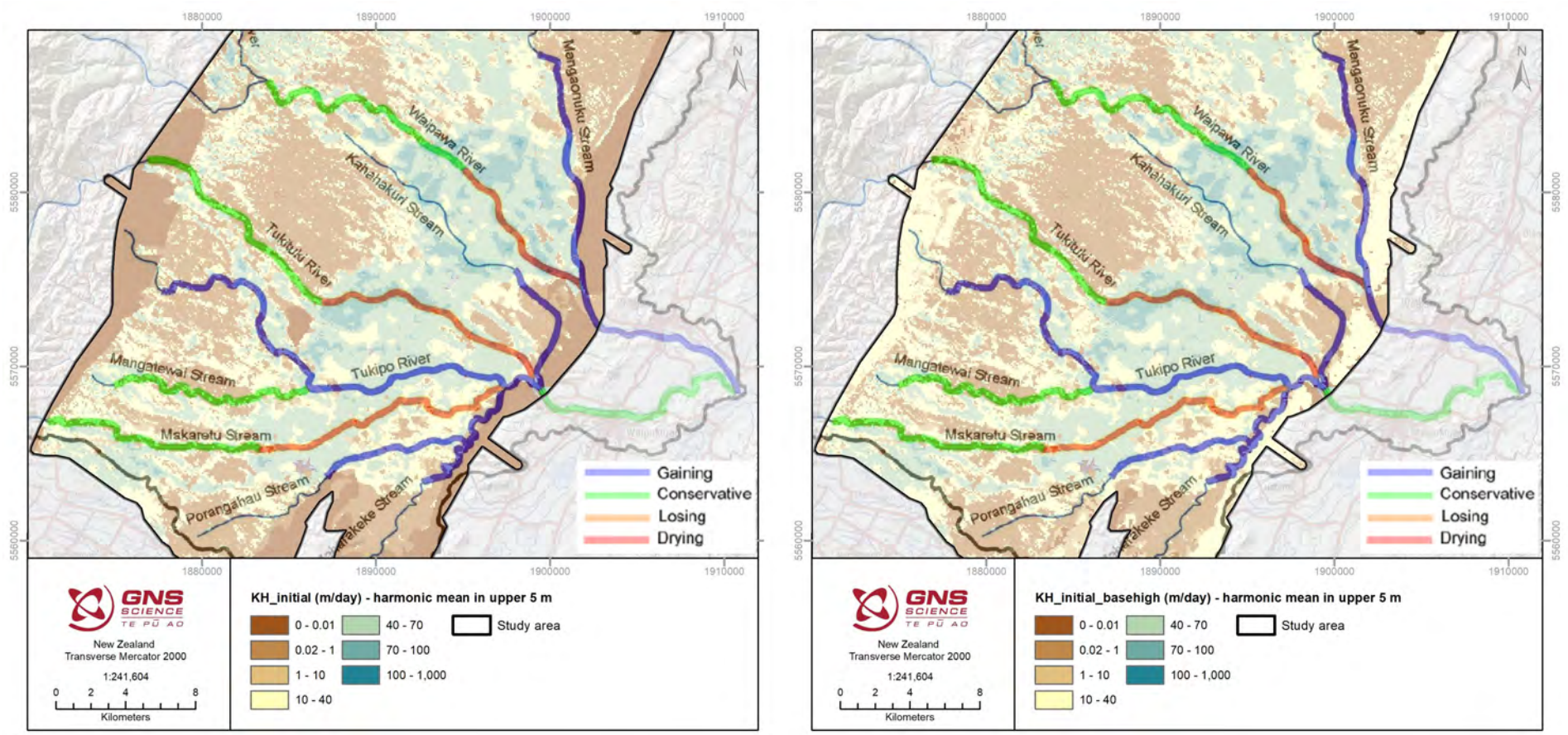

Figure 3.10 Comparison of estimated near-surface permeability with surface water gain and loss estimates from concurrent flow gaugings taken in 2008/2009. (Left) *KH_initial* model, harmonic mean in upper 5 m; (Right) *KH_initial_basehigh* model, harmonic mean in upper 5 m. Figure 20 from Johnson (2011) depicting surface water flow patterns was geo-referenced and placed overtop for comparative purposes.

4.0 DIGITAL DELIVERABLES

All digital maps and data are geo-referenced to coordinate system New Zealand Transverse Mercator (NZTM 2000) and New Zealand Vertical Datum 2020 (NZVD2016).

4.1 3D-Gridded Products

A *.csv* file with all 3D models (see Table 3.1):

- *3D\Ruataniwha_SkyTEM_3Dmodels_V1_2023.csv*

Multi-band raster files for a selection of the 3D models, for numerical groundwater modelling and viewing in GIS. Each multi-band raster contains 500 bands in elevation order, Band 1 = 651 mASL and Band 500 = -349 mASL, with each band consisting of a 2-m-thick vertical slice referenced to the cell centre. This elevation data is included within the metadata of the files:

- *3D\Ruataniwha _SkyTEM_res_V1_2023.tif*
- *3D\Ruataniwha_SkyTEM_resvar_V1_2023.tif*
- *3D\Ruataniwha_SkyTEM_HU_V1_2023.tif*
- *3D\Ruataniwha_SkyTEM_HS_V1_2023.tif*
- *3D\Ruataniwha_SkyTEM_AP_V1_2023.tif*
- *3D\Ruataniwha_SkyTEM_CC_V1_2023.tif*
- *3D\Ruataniwha_SkyTEM_facies_V1_2023.tif*
- *3D\Ruataniwha_SkyTEM_KH_initial_V1_2023.tif*
- *3D\Ruataniwha_SkyTEM_KH_initial_basehigh_V1_2023.tif*
- *3D\Ruataniwha_SkyTEM_KH_unc_V1_2023.tif*

4.2 2D Maps

2D map products provided in raster and GIS polygon formats.

Model area:

- *2D\Ruataniwha_SkyTEM_modelarea.shp*

Aquifer and aquitard thicknesses:

- *2D\Ruataniwha_SkyTEM_aquiferthickness_V1_2023.tif*
- *2D\Ruataniwha_SkyTEM_aquiferthickness_V1_2023.shp*
- *2D\Ruataniwha_SkyTEM_aquiferextent_V1_2023.shp*
- *2D\Ruataniwha_SkyTEM_surficialaquiferthickness_V1_2023.tif*
- *2D\Ruataniwha_SkyTEM_aquiferthickness%_V1_2023.tif*
- *2D\Ruataniwha_SkyTEM_deepaquiferthickness_V1_2023.tif*
- *2D\Ruataniwha_SkyTEM_aquitardthickness_V1_2023.tif*

Near-surface properties – '*' corresponds to one of *res, resvar, CC, KH_initial* and *KH_initial_basehigh* values are provided for both the harmonic mean (*hmean*) and the geometric mean (*gmean*):

- *2D\Ruataniwha_SkyTEM_upper5m_hmean_*_V1_2023.tif*
- *2D\Ruataniwha_SkyTEM_upper10m_hmean_*_V1_2023.tif*
- *2D\Ruataniwha_SkyTEM_upper15m_hmean_*_V1_2023.tif*
- *2D\Ruataniwha_SkyTEM_upper20m_hmean_*_V1_2023.tif*
- *2D\Ruataniwha_SkyTEM_upper30m_hmean_*_V1_2023.tif*
- *2D\Ruataniwha_SkyTEM_upper50m_hmean_*_V1_2023.tif*

Geometric mean and harmonic mean of horizontal hydraulic conductivity models – '*' corresponds to one of *KH_initial, KH_initial_basehigh*:

- *2D\Ruataniwha _SkyTEM_*_gmean_V1_2023.tif*
- *2D\Ruataniwha _SkyTEM_*_hmean_V1_2023.tif*

Geometric mean and harmonic mean of horizontal hydraulic conductivity (*KH_initial*) for the upper 40 m, 75 m and 100 m:

- *2D\Ruataniwha_SkyTEM_upper40m_gmean_KH_initial_V1_2023.tif*
- *2D\Ruataniwha_SkyTEM_upper75m_gmean_KH_initial _V1_2023.tif*
- *2D\Ruataniwha_SkyTEM_upper100m_gmean_KH_initial _V1_2023.tif*
- *2D\Ruataniwha_SkyTEM_upper40m_hmean_KH_initial_V1_2023.tif*
- *2D\Ruataniwha_SkyTEM_upper75m_hmean_KH_initial _V1_2023.tif*
- *2D\Ruataniwha_SkyTEM_upper100m_hmean_KH_initial _V1_2023.tif*

4.3 Supporting Datasets

A 25 m DEM used for 3D model clipping at the land surface (Sahoo et al. 2023):

- *Supporting\RuataniwhaSkyTEM_DEM_25m.asc*

A Leapfrog viewer file containing the DEM, lithological logs and a selection of the 3D models as block models:

- *Supporting\RuataniwhaSkyTEM_LeapfrogViewer.lfview*

A corrected hydraulic conductivity dataset utilised for the assessment in Section 2.1.7.

- *Supporting\Ruataniwha_SkyTEM_aquifertests_KH.csv*

A colour reference file for webmap display:

- *Supporting\Ruataniwha_webmap_colours.csv*

5.0 CONCLUSIONS AND RECOMMENDATIONS

3D model datasets were combined within a *.csv* file, with x,y,z defining the centre of each grid cell and including the following parameters: *X, Y, Z, top_elev_HU, res, resvar, HU, CF, CF_STD, Cluster, Silhouette_Index, HS_unclipped, HS, facies, AP, aq, CC, K_res, K_CC, K_min, KH_initial, KH_initial_basehigh, KH_unc*. A selection of these models was converted to multi-band raster format for use in numerical groundwater modelling. The 3D models utilise 100 x 100 m grid cells horizontally and 2-m-thick grid cells vertically.

The res and CC models were utilised to provide estimates of K_H. It is important to consider upscaling impacts on K_H, and, as such, the best initial values of K_H to use may differ depending on the groundwater modelling objectives. Sufficient datasets have been provided such that the relationship of K_H to the models could be assessed as part of the numerical modelling construction, initial prior simulation runs and calibration. Model formats and types were developed following discussions with numerical groundwater modellers as to the most useful datasets to refine numerical groundwater models.

Section 2.1.7 demonstrated the value of developing an unbiased dataset of aquifer properties and grain size (sampling the expected range of permeability through the area) to assist with confirming relationships between the models and hydraulic conductivity.

Simplifications of the 3D models to 2D maps assisted with more readily investigating various aspects of the Ruataniwha Plains aquifer system, and comparisons to previous investigations highlighted the benefits of these datasets. Overall, the maps and models developed provide useful information to improve the understanding of the hydrogeological system in the Ruataniwha Plains, support a greater understanding of other datasets, and could be used to guide additional data collection with greater precision.

High resistivity values were found at locations of the Tukipo Aquitard/Aquiclude, indicating an insufficient volume of clay material to reduce the resistivity. This could possibly occur due to the binding material consisting of pumice-derived fine material (silica-rich), primarily in the reworked old terraces, which are the ‘cemented’ gravels of the aquitard. The models in this report support the Brown (2002) conclusion that the Tukipo Aquitard/Aquiclude is unlikely to be a valid unit for aquifer grouping, and the extent and significance of this unit may currently be over-stated; however, further investigations may be needed to confirm the resistivity, mineralogical and hydrogeological character of any fine cementing material in the area.

New data in the future that could be used to refine these models include:

- Targeted drilling of the Tukipo Aquitard/Aquiclude and associated analysis, such as clay mineralogy, grain-size analysis and direct resistivity measurements on samples, could assist determining if this is a significant hydrogeological feature that is not being resolved by resistivity variations.
- New resistivity data, for example from ground-based surveys, could be used to fill in gaps within the interpolated resistivity model, which could subsequently result in different subsequent interpretive models.
- New borehole data could be used to revise the HU, HS and CC models.
- New grain-size analyses could be used to further validate the HS and CC models.
- Further information on hydraulic properties and grain size could be used to refine K_H models.
- All of the above could be used to refine the 2D map products.

It is not considered of significant value to revise models on the arrival of a small amount of additional data; however, it should be considered if any significant data collection campaigns are undertaken. Without significant data collection campaigns, possibly a 10-year review would be a suitable time horizon for sufficient additional data to have been collected for there to be value in reviewing and revising models. Additional information that would be of value to improving the quality of modelling includes GPS-located borehole information with high-quality lithological logs and screen location information.

Local studies could refine models through closer interrogation and refinement of datasets for specific local applications.

6.0 ACKNOWLEDGEMENTS

This work has been jointly funded by the New Zealand Government's Provincial Growth Fund, Hawke's Bay Regional Council and GNS Science's Strategic Science Investment Fund (Ministry of Business, Innovation & Employment).

Thank you to Simon Harper of Hawke's Bay Regional Council and Jeff Smith (previously at Hawke's Bay Regional Council) for their contributions to this project. Thank you to Amanda Langley of Project Haus for project management support.

Thank you to Chris Worts for business partnerships support. Thank you to Catherine Moore, Brioch Hemmings, Jeremy White and Mike Taves for discussions relevant to inclusion of these models in numerical groundwater models. Thank you to Tusar Sahoo, Conny Tschritter and Stewart Cameron for providing report reviews.

7.0 REFERENCES

Baalousha H, Goodier CC, Sevicke-Jones GT. 2010. Ruataniwha Basin transient groundwater-surface water flow model. Napier (NZ): Hawke's Bay Regional Council. 103 p. (Technical report, Environmental Management Group; EMT 10/30).

Bouwer H, Rice RC. 1976. A slug test for determining hydraulic conductivity of unconfined aquifers with completely or partially penetrating wells. *Water Resources Research*. 12(3):423–428. https://doi.org/10.1029/WR012i003p00423

Brown LJ. 2002. Ruataniwha Plains groundwater exploration well results. Mountain Creek (AU): LJ Brown. 21 p. + appendices. Prepared for Hawkes Bay Regional Council.

Faunt CC, editor. 2009. Groundwater availability of the Central Valley Aquifer, California. Reston (VA): U.S. Geological Survey. 225 p. Professional Paper 1766.

Foged N. 2022. Hawke's Bay 3D Aquifer Mapping Project: Heretaunga Plains, 3D hydrostratigraphic modelling. Aarhus (DK): Aarhus University HydroGeophysics Group. 27 p. Prepared for Hawke's Bay Regional Council.

Francis D. 2001. Subsurface geology of the Ruataniwha Plains and relation to hydrology. Lower Hutt (NZ): Geological Research Ltd. 28 p. Technical Report. Prepared for Hawke's Bay Regional Council.

Freeze RA, Cherry JA. 1979. Groundwater. Englewood Cliffs (NJ): Prentice-Hall. 604 p.

I-GIS. 2023. GEOScene3D. Risskov (DK): I-GIS; [accessed 2023 July]. https://geoscene3d.com

Johnson K. 2011. Tukituki river hydrological characterisation: supporting information for water allocation. Napier (NZ): Hawke's Bay Regional Council. 28 p. + appendix. (Resource Management Group; EMT 11/05).

Hansen B, Sonnenborg TO, Møller I, Bernth JD, Høyer A-S, Rasmussen P, Sandersen PBE, Jørgensen F. 2016. Nitrate vulnerability assessment of aquifers. *Environmental Earth Sciences*. 75(12):999. https://doi.org/10.1007/s12665-016-5767-2

Harper S. 2018. A review and 3D model of the geology and hydrogeology within the Ruataniwha Basin. Napier (NZ): Hawke's Bay Regional Council. 55 p. (HBRC Report; RM19-241).

Heath RC. 1983. Basic ground-water hydrology. Reston (VA): U.S. Geological Survey. 86 p. Water-Supply Paper 2220.

Hemmings B. 2023. Personal communication. Senior Scientist, Groundwater Modelling; GNS Science, Lower Hutt, NZ.

Hemmings B, Rawlinson ZJ, Moore C, Taves M. In prep. Hawke's Bay 3D Aquifer Mapping Project: Numerical Groundwater Modelling experiments using SkyTEM data in the Heretaunga Plains. Lower Hutt (NZ): GNS Science. Consultancy Report. Prepared for Hawke's Bay Regional Council.

Herpe M, Rawlinson Z. 2023. Hawke's Bay 3D Aquifer Mapping Project: hydrostratigrapic modelling in the Ruataniwha Plains. Lower Hutt (NZ): GNS Science. 13 p. Consultancy Report 2023/102LR. Prepared for Hawke's Bay Regional Council.

Kellett R, Rawlinson Z, Herpe M. 2023. Hawke's Bay 3D Aquifer Mapping Project: interpretation of key boreholes in the Ruataniwha Plains. Lower Hutt (NZ): GNS Science. 11 p. Consultancy Report 2023/36LR. Prepared for Hawke's Bay Regional Council.

Kosinski WK, Kelly WE. 1981. Geoelectric soundings for predicting aquifer properties. *Groundwater*. 19(2):163–171. https://doi.org/10.1111/j.1745-6584.1981.tb03455.x

Lawrence MJF, Herpe M, Kellett RL, Pradel GJ, Sanders F, Coup L, Rawlinson ZJ, Reeves RR, Brakenrig T, Cameron SG, et al. 2022a. Hawke's Bay 3D Aquifer Mapping Project: drilling completion report for borehole 17136 (3DAMP_Well1), Ongaonga-Waipukurau Road, Ruataniwha Plains. Lower Hutt (NZ): GNS Science. 156 p. Consultancy Report 2022/31. Prepared for Hawke's Bay Regional Council.

Lawrence MJF, Herpe M, Pradel GJ, Kellett RL, Coup L, Sanders F, Rawlinson ZJ, Reeves RR, Brakenrig T, Cameron SG, et al. 2022b. Hawke's Bay 3D Aquifer Mapping Project: drilling completion report for borehole 17164 (3DAMP_Well3), Burnside Road, Ruataniwha Plains. Lower Hutt (NZ): GNS Science. 76 p. Consultancy Report 2022/15. Prepared for Hawke's Bay Regional Council.

Lee JM, Begg JG, Bland KJ. 2020. Geological map of the Napier-Hastings urban area. Lower Hutt (NZ): GNS Science. 1 map, scale 1:75,000. (GNS Science geological map; 7a).

Maneewongvatana S, Mount D. 2002. Analysis of approximate nearest neighbor searching with clustered point sets. In: Goldwasser MH, Johnson DS, McGeoch CG, editors. *Data structures, near neighbor searches, and methodology: fifth and sixth DIMACS implementation challenges*. Providence (RI): American Mathematical Society. p. 105–124. (DIMACS series in discrete mathematics and theoretical computer science; 59).

Meilhac C, Reeves RR, Zemansky GM, White PA, Jebbour N. 2009. Field investigation of groundwater-surface water interactions, Ruataniwha Plains. Lower Hutt (NZ): GNS Science. 127 p. (GNS Science report; 2009/23).

Mele M, Bersezio R, Giudici M. 2012. Hydrogeophysical imaging of alluvial aquifers: electrostratigraphic units in the quaternary Po alluvial plain (Italy). *International Journal of Earth Sciences*. 101(7):2005–2025. https://doi.org/10.1007/s00531-012-0754-7

Minsley BJ, Rigby JR, James SR, Burton BL, Knierim KJ, Pace MDM, Bedrosian PA, Kress WH. 2021. Airborne geophysical surveys of the lower Mississippi Valley demonstrate system-scale mapping of subsurface architecture. *Communications Earth & Environment*. 2:article 131. https://doi.org/10.1038/s43247-021-00200-z

Moore C. 2023. Personal communication. Principal Scientist, Groundwater Modelling; GNS Science, Lower Hutt, NZ.

Morgenstern U, van der Raaij RW, Baalousha H. 2012. Groundwater flow pattern in the Ruataniwha Plains as derived from the isotope and chemistry signature of the water. Lower Hutt (NZ): GNS Science. 44 p. (GNS Science report; 2012/23).

Niwas S, Celik M. 2012. Equation estimation of porosity and hydraulic conductivity of Ruhrtal aquifer in Germany using near surface geophysics. *Journal of Applied Geophysics*. 84:77–85. https://doi.org/10.1016/j.jappgeo.2012.06.001

[PDP] Pattle Delamore Partners. 1999. Ruataniwha Plains conceptual hydrogeological model. Auckland (NZ): PDP. Technical report EMT 99/3.

[PDP] Pattle Delamore Partners. 2018. Ruataniwha Aquifer properties and mapping. Auckland (NZ): PDP. 34 p. Prepared for Hawke's Bay Regional Council.

Perwick A, Woodhouse C. 2014. Heretaunga Plains transmissivity and storativity maps. Christchurch (NZ): Pattle Delamore Partners Ltd. 25 p. + appendices. Report RM16-25. Prepared for Hawke's Bay Regional Council.

Ponzini G, Ostroman A, Molinari M. 1984. Empirical relation between electrical transverse resistance and hydraulic transmissivity. *Geoexploration*. 22(1):1–15. https://doi.org/10.1016/0016-7142(84)90002-4

Purvance DT, Andricevic R. 2000. On the electrical-hydraulic conductivity correlation in aquifers. *Water Resources Research*. 36(10):2905–2913. https://doi.org/10.1029/2000WR900165

Rakowski P, Knowling MJ. 2018. Heretaunga aquifer groundwater model: development report. Napier (NZ): Hawke's Bay Regional Council. 182 p. HRBC Report RM18-14.

Rawlinson Z. 2013. A review of the most effectual and economical geophysical techniques for characterising groundwater within New Zealand. Lower Hutt (NZ): GNS Science. 90 p. (GNS Science report; 2013/38).

Rawlinson Z. 2023. Hawke's Bay 3D Aquifer Mapping Project: 3D hydrogeological models from SkyTEM data in the Heretaunga Plains. Wairakei (NZ): GNS Science. 69 p. Consultancy Report 2023/57. Prepared for Hawke's Bay Regional Council.

Rawlinson ZJ, Reeves RR, Westerhoff RS, Foged N, Pederson JB, Kellett RL. 2022. Hawke's Bay 3D Aquifer Mapping Project: Ruataniwha Plains SkyTEM data processing and resistivity models. Wairakei (NZ): GNS Science. 79 p. Consultancy Report 2022/38. Prepared for Hawke's Bay Regional Council.

Rawlinson ZJ, Sahoo TR, Kellett RL, Cameron SG. In press. Hawke's Bay 3D Aquifer Mapping Project: hydrogeological interpretation of the SkyTEM-derived resistivity models within the Poukawa and Otane basins. Wairakei (NZ): GNS Science. 107 p. Consultancy Report 2021/12.

Sahoo T, Rawlinson Z, Kellett R. 2023. Hawke's Bay 3D Aquifer Mapping Project: delineation of hydrogeological basement within the Ruataniwha Plains from SkyTEM-derived resistivity models. Lower Hutt (NZ): GNS Science. 10 p. Consultancy Report 2023/39LR. Prepared for Hawke's Bay Regional Council.

SkyTEM Australia Pty Ltd. 2020. Acquisition and processing report: SkyTEM helicopter EM survey, Hawkes Bay, NZ. Malaga (AU): SkyTEM Australia Pty Ltd. 33 p. Report AUS 10056. Prepared for Hawke's Bay Regional Council.

Slater L. 2007. Near surface electrical characterization of hydraulic conductivity: from petrophysical properties to aquifer geometries – a review. *Surveys in Geophysics*. 28:169–197. https://doi.org/10.1007/s10712-007-9022-y

Tschritter C, Herpe M, Kellett RL, Rawlinson ZJ, Arnot MJ, Griffin AG, Lawrence MJF. 2022. Hawke's Bay 3D Aquifer Mapping Project: Ruataniwha Plains data and model inventory. Wairakei (NZ): GNS Science. 111 p. Consultancy Report 2022/76. Prepared for Hawke's Bay Regional Council

Urish DW. 1981. Electrical resistivity – hydraulic conductivity relationships in glacial outwash aquifers. *Water Resources Research*. 17(5):1401–1408. https://doi.org/10.1029/WR017i005p01401

Virtanen P, Gommers R, Oliphant TE, Haberland M, Reddy T, Cournapeau D, Burovski E, Peterson P, Weckesser W, Bright J, et al. 2020. SciPy 1.0: fundamental algorithms for scientific computing in Python. *Nature Methods*. 17(3):261–272. https://doi.org/10.1038/s41592-019-0686-2

www.gns.cri.nz

Principal Location

1 Fairway Drive, Avalon
Lower Hutt 5010
PO Box 30368
Lower Hutt 5040
New Zealand
T +64-4-570 1444
F +64-4-570 4600

Other Locations

Dunedin Research Centre
764 Cumberland Street
Private Bag 1930
Dunedin 9054
New Zealand
T +64-3-477 4050
F +64-3-477 5232

Wairakei Research Centre
114 Karetoto Road
Private Bag 2000
Taupo 3352
New Zealand
T +64-7-374 8211
F +64-7-374 8199

National Isotope Centre
30 Gracefield Road
PO Box 30368
Lower Hutt 5040
New Zealand
T +64-4-570 1444
F +64-4-570 4657